AD-A175 450 TUNABLE MOLECULAR LASERS(U) ILLINOIS UNIV AT URBANA 1/1
DEPT OF ELECTRICAL AND COMPUTER ENGINEERING
J G EDEN ET AL SEP 86 UILU-ENG-86-2556 ARO-20802 7-PH
UNCLASSIFIED DAAG29-83-K-0108 F/G 20/5 NL

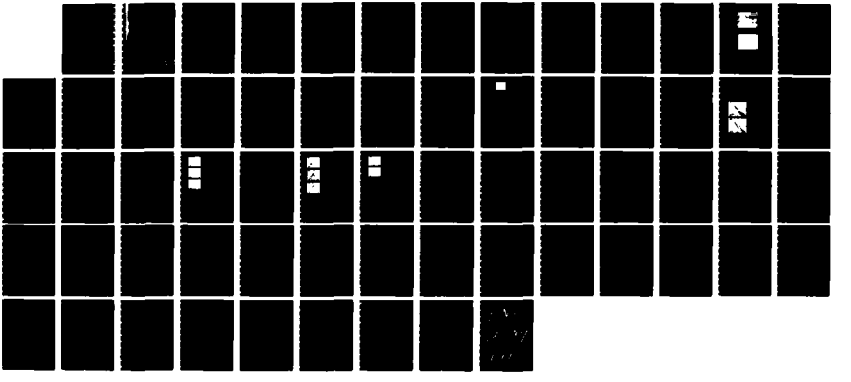

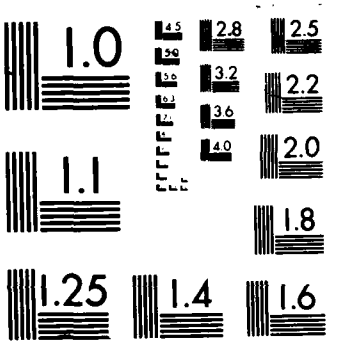

TUNABLE MOLECULAR LASERS

FINAL REPORT

J. G. EDEN

SEPTEMBER 1986

Dr. B. D. Guenther
Physics Division
U. S. Army Research Office
P. O. Box 12211
Research Triangle Park, NC 27709-2211

Contract No. DAAG 29-83-K-0108

Department of Electrical and Computer Engineering
University of Illinois at Urbana-Champaign
1406 W. Green St.
Urbana, IL 61801

UILU-ENG-86-2556

TUNABLE MOLECULAR LASERS

FINAL REPORT

J. G. EDEN

SEPTEMBER 1986

Dr. B. D. Guenther
Physics Division
U. S. Army Research Office
P. O. Box 12211
Research Triangle Park, NC 27709-2211

Contract No. DAAG 29-83-K-0108

Department of Electrical and Computer Engineering
University of Illinois at Urbana-Champaign
1406 W. Green St.
Urbana, IL 61801

UNCLASSIFIED

SECURITY CLASSIFICATION OF THIS PAGE (When Data Entered)

AD-A175450

REPORT DOCUMENTATION PAGE		READ INSTRUCTIONS BEFORE COMPLETING FORM
1. REPORT NUMBER ARO 20002.7-PH	2. GOVT ACCESSION NO. N/A	3. RECIPIENT'S CATALOG NUMBER N/A
4. TITLE (and Subtitle) TUNABLE MOLECULAR LASERS		5. TYPE OF REPORT & PERIOD COVERED 8-1-83 - 7-31-86 FINAL REPORT
		6. PERFORMING ORG. REPORT NUMBER UILU-ENG-86-2556
7. AUTHOR(s) J. G. EDEN		8. CONTRACT OR GRANT NUMBER(s) DAAG 29-83-K-0108
9. PERFORMING ORGANIZATION NAME AND ADDRESS Department of Elec. and Computer Engg. Univ. of Illinois at Urbana-Champaign 1406 W. Green St., Urbana, IL 61801		10. PROGRAM ELEMENT, PROJECT, TASK AREA & WORK UNIT NUMBERS N/A
11. CONTROLLING OFFICE NAME AND ADDRESS U. S. Army Research Office Post Office Box 12211 Research Triangle Park, NC 27709		12. REPORT DATE September 1986 13. NUMBER OF PAGES 61
14. MONITORING AGENCY NAME & ADDRESS(if different from Controlling Office)		15. SECURITY CLASS. (of this report) UNCLASSIFIED 15a. DECLASSIFICATION DOWNGRADING SCHEDULE

16. DISTRIBUTION STATEMENT (of this Report)

Approved for public release; distribution unlimited.

17. DISTRIBUTION STATEMENT (of the abstract entered in Block 20, if different from Report)

NA

18. SUPPLEMENTARY NOTES

The view, opinions, and/or findings contained in this report are those of the author(s) and should not be construed as an official Department of the Army position, policy, or decision, unless so designated by other documentation.

19. KEY WORDS (Continue on reverse side if necessary and identify by block number)

laser, visible, tunable, mercury bromide, dye vapor, optically pumped

20. ABSTRACT (Continue on reverse side if necessary and identify by block number)

Experiments are described in which the potential of dye vapors and HgBr as tunable visible lasers has been investigated. As a result of this three year effort, several significant results have been obtained. The $B^2\Sigma \leftarrow X^2\Sigma$ absorption band of HgBr at 350 nm has been obtained and a near-UV, optically-pumped HgBr laser has been demonstrated. The 502 nm HgBr laser has also been successfully flashlamp-pumped. Charge transfer absorption from $HgBr(B^2\Sigma)$ at $\lambda \sim 447$ nm has been observed and the upper state tentatively identified.

(over)

DD FORM 1 JAN 73 1473 EDITION OF 1 NOV 65 IS OBSOLETE

UNCLASSIFIED

SECURITY CLASSIFICATION OF THIS PAGE (When Data Entered)

TABLE OF CONTENTS

		Page
I.	INTRODUCTION	2
II.	DYE VAPOR EXPERIMENTS: POPOP AND COUMARIN 6	3
III.	HgBr ABSORPTION STUDIES	4
IV.	OPTICALLY PUMPED HgBr LASER	10
V.	SUMMARY	12
VI.	APPENDIX: Copies of ARO-Supported Publications*	13

*Each publication in Appendix has its own pagination.

FINAL REPORT

1. ARO PROPOSAL NUMBER: P-20002-PH

2. PERIOD COVERED BY REPORT: August 1, 1983 through July 31, 1986

3. TITLE OF PROPOSAL: Tunable Molecular Lasers

4. CONTRACT OR GRANT NUMBER: DAAG 29-83-K-0108

5. NAME OF INSTITUTION: University of Illinois

6. AUTHORS OF REPORT: J. G. Eden

7. LIST OF MANUSCRIPTS SUBMITTED OR PUBLISHED UNDER ARO SPONSORSHIP DURING THIS CONTRACT, INCLUDING JOURNAL REFERENCES:

D. P. Greene and J. G. Eden, "Injection locking and saturation intensity of a cadmium iodide laser," Opt. Lett. 10, pp. 59-61 (1985).
D. P. Greene and J. G. Eden, "Origin of the 454 nm bound → free absorption band of cadmium monoiodide (^{114}CdI)," J. Chem. Phys. 82, pp. 702-708 (1985).
J. G. Eden (Book Review), J. Opt. Soc. Am. B 2, p. 390 (1985).
D. P. Greene and J. G. Eden, "Transient absorption in a cadmium monoiodide laser discharge," Opt. Comm. 53, pp. 263-268 (1985).
D. P. Greene, K. P. Killeen and J. G. Eden, "$X^2\Sigma \rightarrow B^2\Sigma$ absorption band of HgBr: Optically-pumped 502 nm laser," Appl. Phys. Lett. 48, pp. 1175-1177 (1986).
J. G. Eden and K. P. Killeen, "I_2 amplifier in the green," Proc. SPIE 476, pp. 34, 35 (1984).
K. P. Killeen and J. G. Eden, "Coupling of the green (506 nm) and ultraviolet (342 nm) emission bands of I_2," J. Opt. Soc. Am. B 2, pp. 430-432 (1985).
D. P. Greene, K. P. Killeen and J. G. Eden, "Excitation of the HgBr $B^2\Sigma^+_{1/2} \rightarrow X^2\Sigma^+_{1/2}$ band in the ultraviolet," J. Opt. Soc. Am. B (to be published).

8. SCIENTIFIC PERSONNEL SUPPORTED BY THIS PROJECT AND DEGREES AWARDED DURING THIS REPORTING PERIOD:

J. G. Eden, K. P. Killeen, D. P. Greene, R. W. Herrick

Degrees Awarded:
D. P. Greene, Ph.D. in Electrical Engineering January, 1985.
K. P. Killeen, Ph.D. in Electrical Engineering October, 1985.
R. W. Herrick, M.S. in Electrical Engineering October, 1986.

J. G. Eden
Department of Electrical and Computer Engineering
University of Illinois
Urbana, IL 61801

I. INTRODUCTION

Over the last three years, the Army Research Office supported experimental work in laser physics here at the University of Illinois. The goal of this research program was two-fold: 1) to develop new sources of tunable coherent radiation in the visible and ultraviolet and 2) to better understand the fundamental processes occuring in existing sources and particularly those that show promise for improvement in efficiency and output power.

This work proved to be very fruitful in both areas. Specifically, the following accomplishments were realized during the contract period:

1) Stable, streamer-free discharges were obtained in coumarin 6 and POPOP vapors - glows were sustained at PRF's of 1-5 Hz for several hours with no noticeable deterioration in fluorescence intensity from the active region.
2) Excited state absorption of the cadmium monoiodide (CdI) and mercury-bromide (HgBr) molecules was observed and spectroscopically assigned for the first time.
3) The X → B absorption band of HgBr was observed.
4) An HgBr laser at 502 nm, optically pumped at 351 nm (XeF) or 355 nm (3 X Nd:YAG), was demonstrated.
5) A flashlamp-pumped HgBr laser was demonstrated.

Each of these results will be described briefly in the following sections.

II. DYE VAPOR EXPERIMENTS: POPOP AND COUMARIN 6

One of the goals of this research program was to investigate the excitation of dye vapors in a UV-preionized, transverse discharge device. After considerable effort and several iterations, the necessary discharge cell was successfully built and demonstrated. This device has an active length of 50 cm, an equivalent series inductance of ~ 85 nH and is capable of sustained operation at 450° C. For a buffer gas pressure of ~ 1 atm, the cell routinely produces a specific power loading of the active medium of 2 - 5 MW-cm^{-3}.

In experiments with the dye vapors it was found that stable and intense discharges in POPOP and coumarin 6 vapor could be obtained. For coumarin 6, for example, the fluorescence risetime was < 20 ns. Two interesting and encouraging results of this work were that the discharges were completely streamer-free and, secondly, that dye fragmentation was not as serious a problem as anticipated. At a discharge PRF of 1 - 5 Hz, the dye fluorescence did not noticeably deteriorate, even after hours of operation.

Preliminary gain/absorption experiments on coumarin 6 vapor with an Ar^+ laser probe revealed only net absorption. It should be noted, however, that the only wavelengths available from the Ar^+ laser lie to the blue of where one would expect significant gain ($\lambda \sim 540$ nm). These experiments are continuing with a widely tunable probe.

III. HgBr ABSORPTION STUDIES

A broad-band absorption probe technique developed in this laboratory has been applied to examining the structure of the HgBr molecule, and particularly as it bears on obtaining an efficient, tunable visible laser. Figure 1 shows the gain/absorption spectrum of the HgBr molecule as obtained in a discharge in Ne, N_2 and $HgBr_2$ vapor. A highly structured absorption band, which peaks at $\lambda \sim 447$ nm, is clearly observed in the blue. As will be shown later, this band is the analog of the CdI charge transfer band previously observed in the visible.

The absorption spectra for $427 \leq \lambda \leq 457$ nm and for time delays of 0 and 450 ns (after firing the HgBr discharge) are compared in Fig. 2. The spectral region for this figure is the same as that of the boxed portion of Fig. 1. The data are consistent with a relatively rapid depopulation of the B state, in part due to the large B → X transition probability. These data suggest that the peak at 447 nm is due to absorption from the HgBr B state, terminating on a previously unobserved and, as of yet, unidentified upper level. An aside that is important insofar as tunable lasers are concerned is that, at the same time these measurements were made, we discovered that the HgBr B → X band exhibits gain as far to the blue as 469 nm! Therefore, this oscillator is potentially tunable over as much as ~ 30 nm.

The identity of the HgBr blue band was also confirmed by exciting the active medium with a dye laser pulse of wavelength $444 \leq \lambda \leq 454$ nm while at the same time monitoring the gain at 502 nm (peak of B → X band). As shown by Figure 3, when the wavelength of the first dye laser pulse coincided with one of the 447 nm band absorption peaks of Figure 2, a strong suppression in the 502 nm gain waveform was observed. At other wavelengths (between the absorption peaks or outside the band), little or no effect on the 502 nm gain was detectable. Of

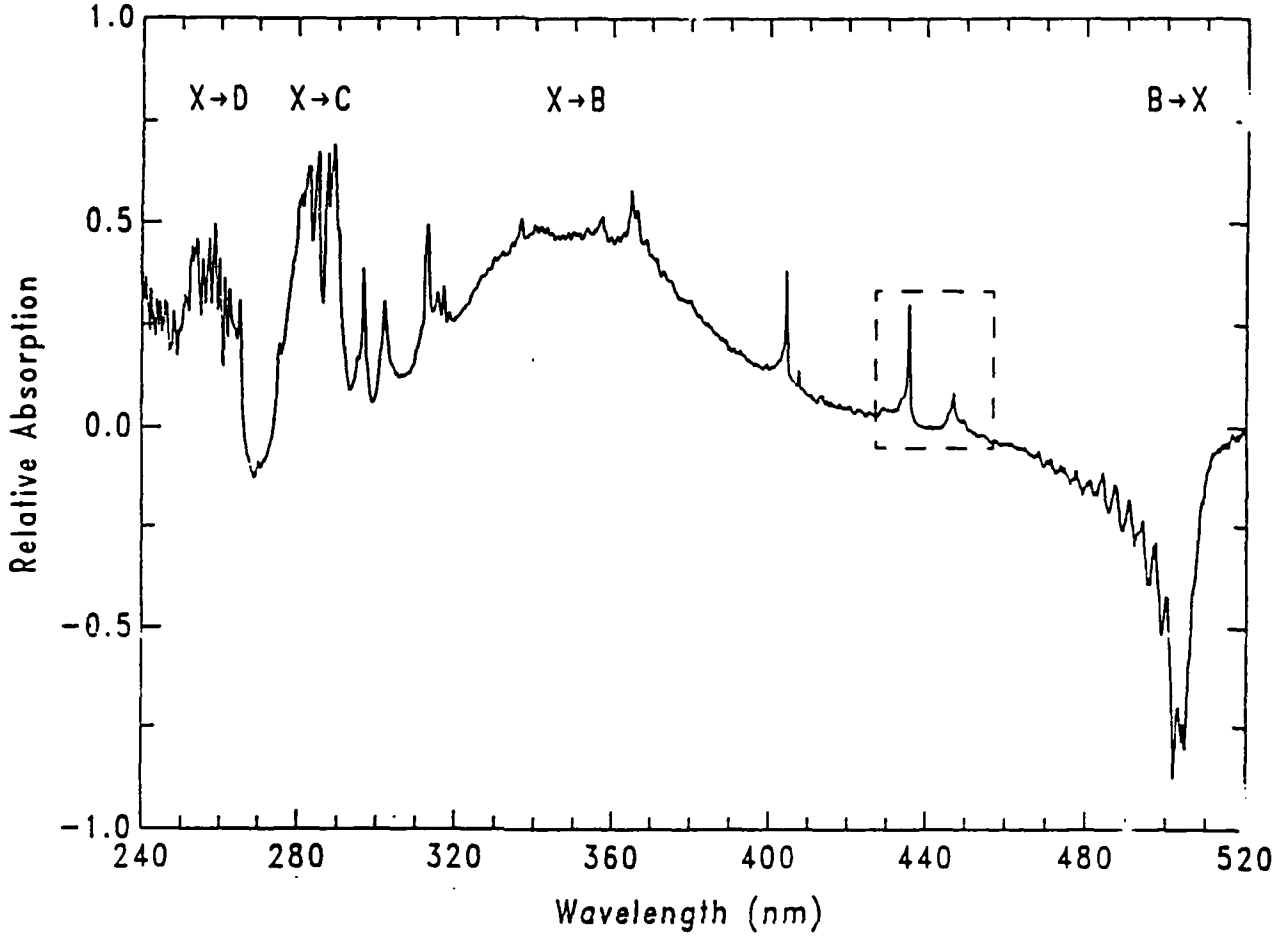

Figure 1. Absorption spectrum of HgBr.

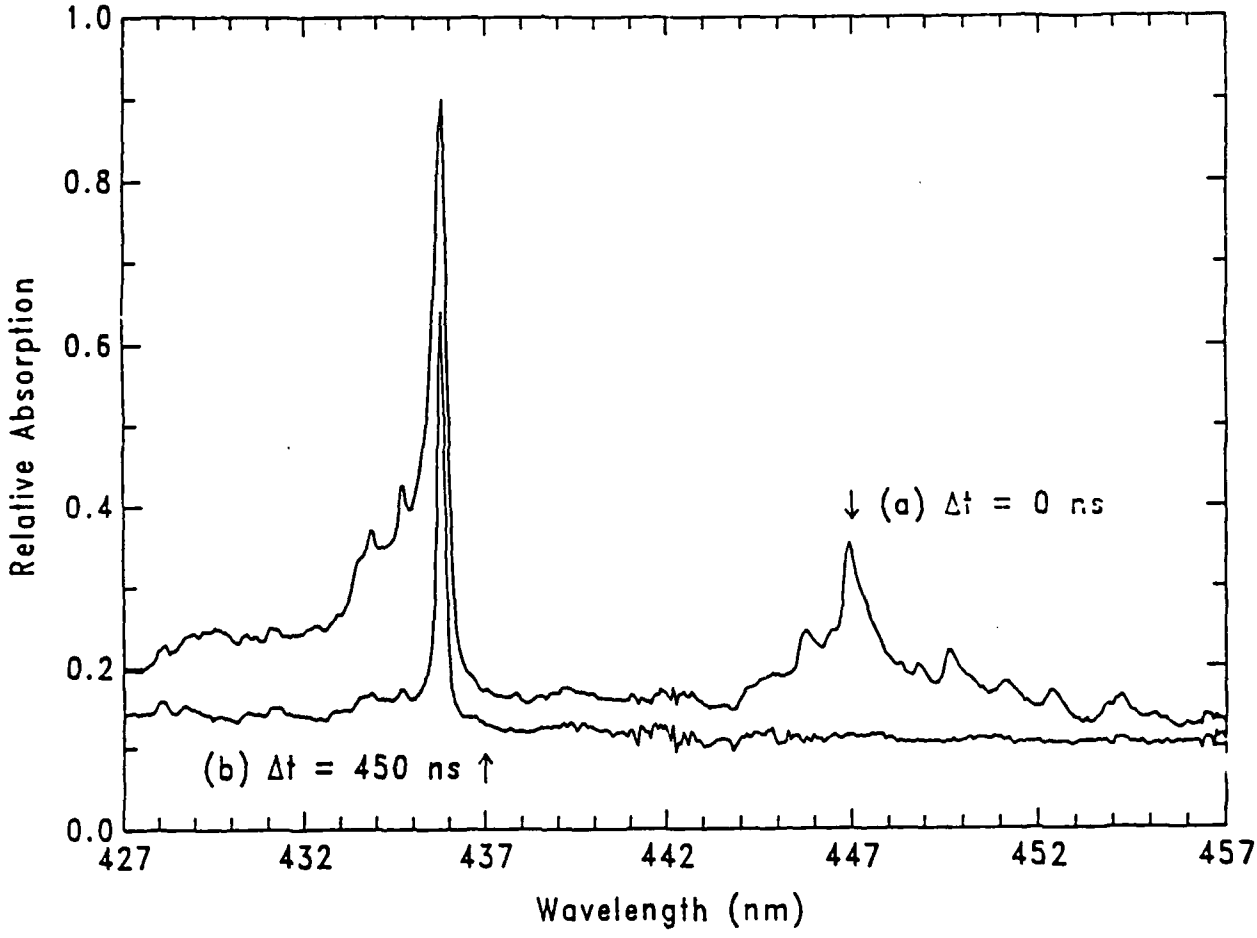

Figure 2. Absorption spectra at time delays of (a) 0 and (b) 450 ns. HgBr B-state is effectively depopulated in (b), while Hg 435.8 nm line is relatively strong.

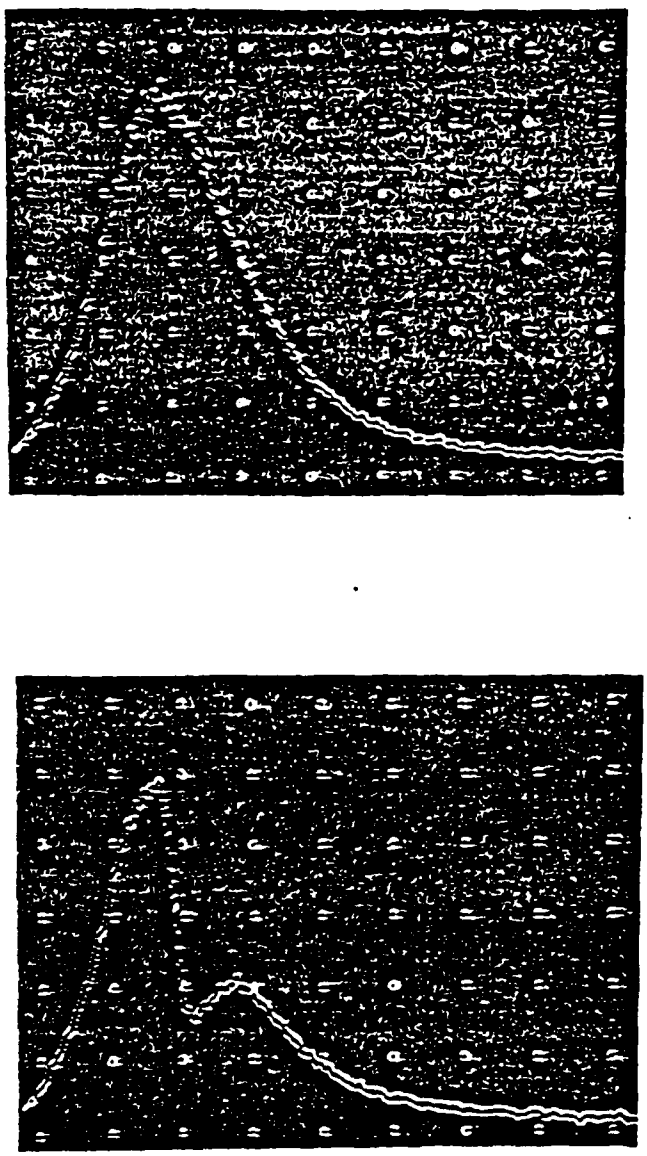

Figure 3. (Top) Gain at 502 nm in HgBr laser discharge; (Bottom) Suppression of gain when laser plasma is irradiated at 446.98 nm. Peak suppression is 70% and the dye laser pulse was timed to arrive at the point of peak gain. Time base: 50 ns/div.

course, the strongest suppression was observed when λ = 446.98 nm and the gain suppression at other absorption peaks is proportional to the absorption strength. The variation of B → X gain suppression with probing wavelength is illustrated in Fig. 4.

By varying the laser fluence at $\lambda \sim 447$ nm and measuring the transmitted blue intensity, the "saturation intensity" of the HgBr excited state absorption band was measured to be 710 kW - cm^{-2}. Similarly, the absorption cross-section at 446.98 nm is $3 \cdot 10^{-17}$ cm^2. Finally, it should be mentioned that the structure of the band shown in Figure 2 is consistent with an HgBr absorption band originating from the B state - the energy spacing between alternate peaks in the blue absorption band is close to the known ω_e for $B^2\Sigma(\sim 139\ cm^{-1})$.

In summary, excited state absorption in CdI and HgBr has been observed for the first time though the existence of such bands had been predicted theoretically for at least a decade. Details of our experimental results can be found in the attached reprint which was published in the Journal of Chemical Physics.

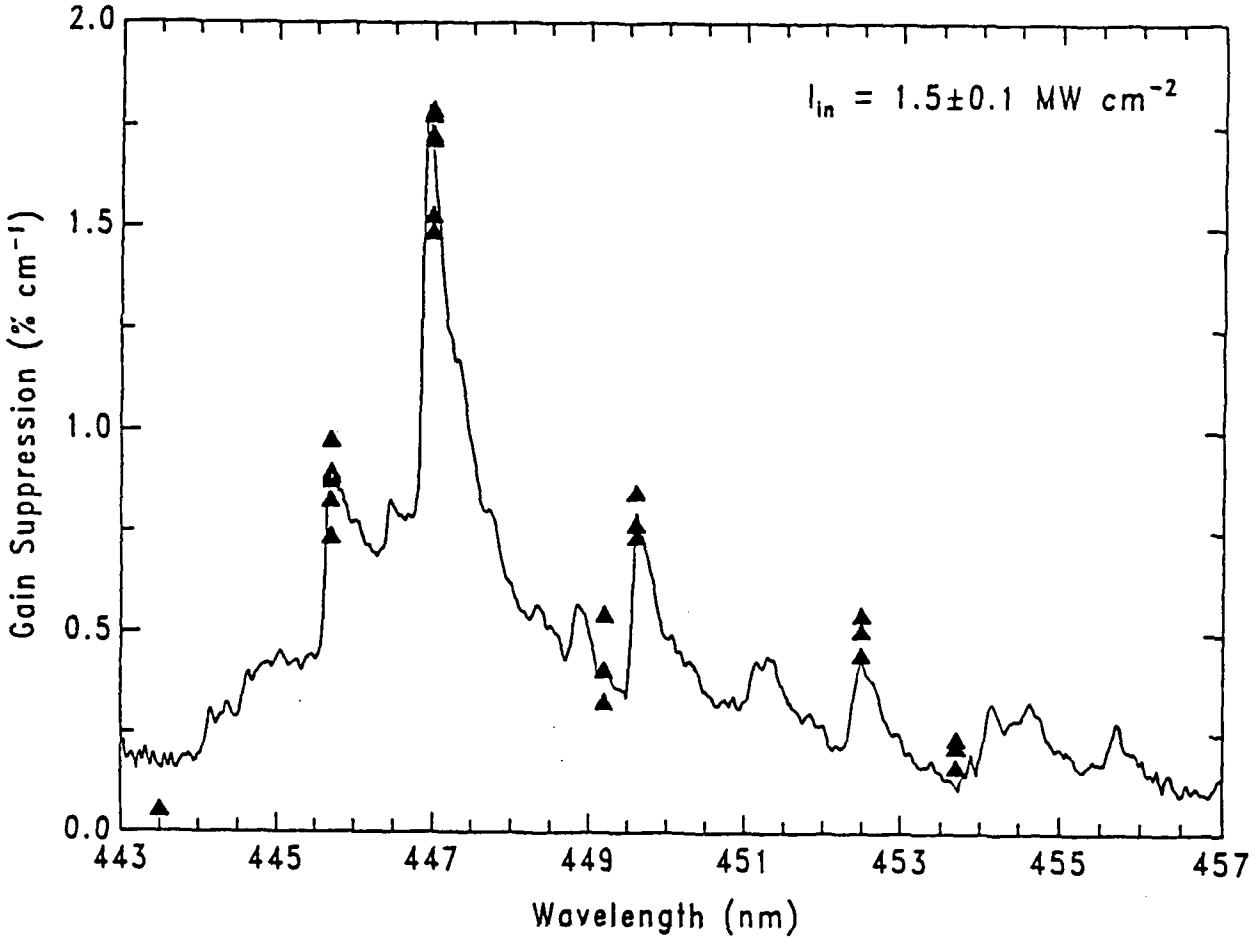

Figure 4. Results of gain suppression measurements (triangles) in comparison to the absorption spectrum.

IV. OPTICALLY PUMPED HgBr LASER

During this contract period, we uncovered a simple and efficient way to pump the HgBr laser - a method which we believe is amenable to CW operation. In the course of examining the transient absorption spectrum for the HgBr discharge laser, we unexpectedly observed the HgBr X → B absorption band. Figure 5 shows the X → B absorption spectrum of HgBr that was measured with a pulsed lamp and OMA in the afterglow of a discharge pumped HgBr laser based on dissociation of $HgBr_2$.

Because of the relatively low photon energies required to access the $B^2\Sigma$ state from ground (~ 3.5 eV), one can quickly envision an optically-pumped HgBr laser having a high quantum efficiency (2.5 eV/3.5 eV = 71%). Preliminary experiments to explore this possibility have been conducted. An ~ 8 ns pulse from a frequency tripled, Q-switched Nd:YAG (λ = 355 nm) or XeF laser was directed along the axis of a discharge-pumped HgBr laser (active length of 50 cm; $He/N_2/HgBr_2$ gas mixture). Fired by itself, the discharge produces an ~ 40 ns FWHM HgBr laser pulse. Once the 355 nm laser pulse arrives, a second HgBr pulse is generated having a width of ~ 10 ns. The efficiency for converting XeF radiation (λ = 351 nm) into blue-green output is 23% which corresponds to a photon conversion efficiency of approximately 1/3. These data are extremely reproducible.

The obvious match between the peak in the X → B absorption spectrum of Figure 5 and the spectral output of a xenon flashlamp prompted us to explore the possibility of a pulsed, coaxial flashlamp-pumped HgBr laser. Several milligrams of natural abundance $HgBr_2$ and 760 Torr of argon buffer gas were contained in a quartz cell having Surpasil quartz Brewster windows. Lasing was obtained with a high-Q cavity (1% output coupling) - larger couplings have not yet been tried. A pulse of ~ 280 ns FWHM is produced.

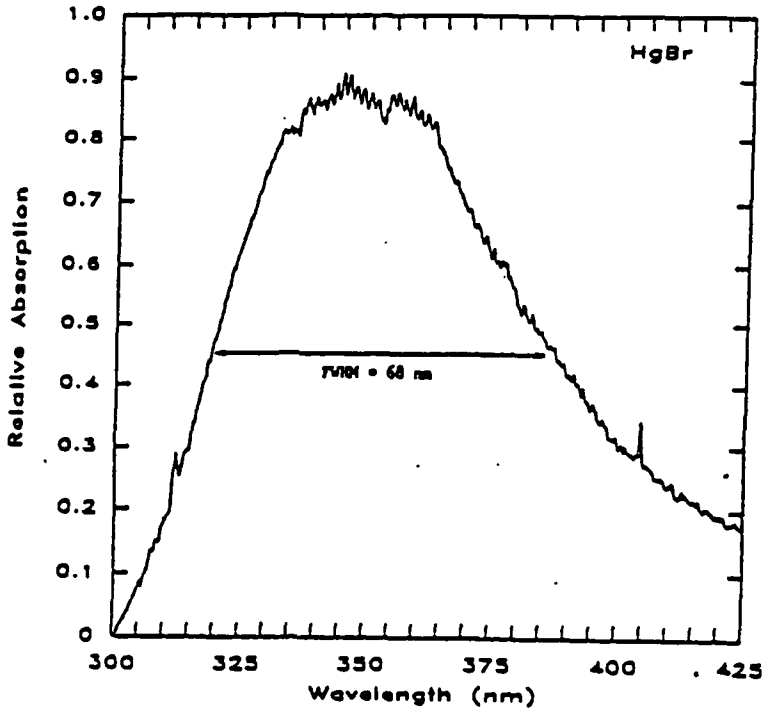

Figure 5. Ground state HgBr absorption spectrum in the near-ultraviolet that was recorded in the afterglow of a pulsed HgBr laser discharge.

V. SUMMARY

Several significant accomplishments have been realized during the life of this contract. The HgBr experiments show that this molecule is particularly promising as an efficient source of tunable, CW visible radiation.

The Appendix contains copies of all of the papers published (or to be published) with ARO support.

VI. APPENDIX: Copies of ARO-Supported Publications

Reprinted from SPIE Vol. 476—Excimer Lasers, Their Applications, and New Frontiers in Lasers

I_2 amplifier in the green

J. G. Eden and K. P. Killeen

University of Illinois
1406 W. Green Street, Urbana, Illinois 61801

Abstract

The collisional coupling between the green ($\lambda \sim 505$ nm) and UV (342 nm) bands of I_2 has been examined in electron beam-pumped mixtures of Ar and hydrogen iodide (HI). The strong interaction between the two is evidenced by the large suppression (> 40%) of the 342 nm $D' \rightarrow A'$ fluorescence that is observed when a green dye laser pulse ($\lambda \sim 503$ nm) of $I \geq 4$ MW - cm^{-2} is injected into the medium.

Recently, gain on the green (505 nm) excimer band of I_2 in electron beam-pumped mixtures of Ar (or Ne) and hydrogen iodide was reported.[1] At the time, it was noted that peak gain coefficients of ~ 1.2 % - cm^{-1} were observed at $\lambda \sim 506$ nm despite the fact that the ultraviolet band at 342 nm was superfluorescing. Secondly, preliminary experimental observations suggested that the two bands were collisionally coupled (indeed, earlier workers suggested that the two bands shared a common upper state). If the two bands strongly interact with one another, then, of course, the gain on the green band could be considerably enhanced by suppressing entirely the UV emission.

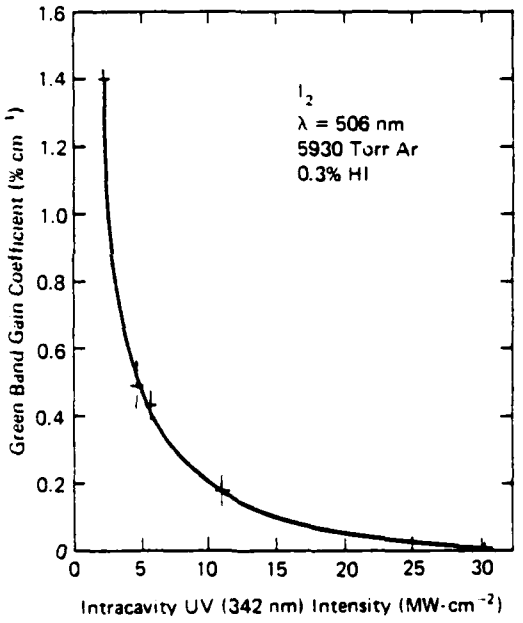

Figure 1. Variation of the green band gain coefficient with the ultraviolet intensity in the optical cavity. Note the steep slope of the curve at the lowest UV intensity studied (1.8 MW - cm^{-2}).

Interest in the green band of I_2 stems from the large spectral breadth over which an oscillator could potentially be tuned (full width of band ~ 15 nm), as well as the position of the band in the visible. Few excimer lasers exist outside the ultraviolet with the $C \rightarrow A$ band of XeF, Xe_2Cl and Kr_2F being obvious exceptions.

The purpose of the work briefly described here was to investigate the degree of competition between the I_2 green and UV bands. The experimental apparatus is quite similar to that described in Reference 1. A cylindrical electron beam diode of 20 cm gain length was used to excite the mixtures of argon and hydrogen iodide. The only addition is an excimer laser-pumped dye laser which was used, in one set of experiments, to saturate the green transition.

A simple way to examine the coupling between the upper energy levels for the green and UV bands of I_2 is to artificially increase the UV flux in the medium by installing an optical cavity around the e-beam cell. By varying the reflectivities of the mirrors involved, the Q of the cavity and, hence, the magnitude of the circulating ultraviolet intensity could also be changed. As illustrated in Figure 1, increasing the 342 nm intensity induces a dramatic drop in the gain coefficient measured at 506 nm with a pulsed dye laser (CMX-4). Amplification in the green has vanished for $I_{342\ nm} \sim 30$ MW - cm^{-2}. Note also the steep slope of the smooth curve drawn through the data at the lowest UV intensity examined (1.8 MW - cm^{-2}). This also strongly suggests that the small signal gain coefficient for the green band is considerably larger than the values measured to date.

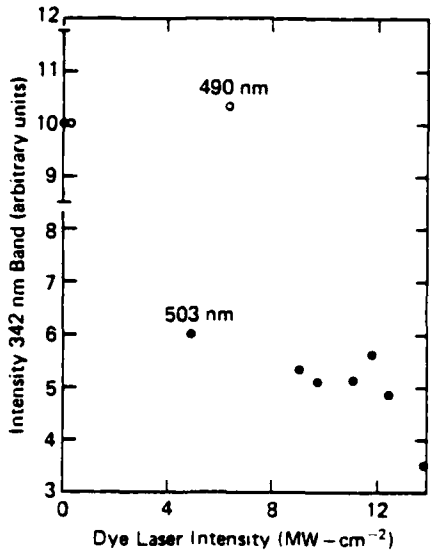

Figure 2. Dependence of the peak UV intensity on the intensity of a dye laser pulse injected along the axis of the e-beam diode.

In a second set of experiments, a green dye laser pulse was injected into the gain medium at the peak of the green gain pulse. The effect of this injected radiation on the UV emission is shown in Figure 2. Again, the result is obvious as the UV intensity drops by almost a factor of two (from its $I_{green} = 0$ value) for an injected beam intensity (503 nm) of ~ 5 MW - cm^{-2}. If, on the other hand, one tunes the dye laser to a point just outside the I_2 excimer band (i.e., 490 nm), such a dramatic effect is not observed.

In summary, strong suppression of either the I_2 D' → A' UV or green excimer bands is observed as the intensity is increased on the other transition. The low intensities required to observe this effect indicate that the degree of collisional coupling between the two upper states involved is high.

Acknowledgments

This work was supported by the Army Research Office (B. Guenther under Grant DAAG 29-83-K-0108 and the National Science Foundation (J. Aller) under Grant ECS 83-09641.

Reference

1. K. P. Killeen and J. G. Eden, Appl. Phys. Lett. 43, 539, (1983).

Reprinted from Journal of the Optical Society of America B, Vol. 2, page 430, March, 1985

Coupling of the green (506-nm) and ultraviolet (342-nm) emission bands of I_2

K. P. Killeen and J. G. Eden

University of Illinois, Urbana, Illinois 61801

Received July 31, 1984; accepted October 19, 1984

Collisional coupling between the electronic excited states of I_2 that are responsible for the green and ultraviolet ($D' \rightarrow A'$) bands of the molecule (centered at 506 and 342 nm, respectively) has been studied in electron-beam-pumped mixtures of argon and hydrogen iodide (HI). The dependence of the temporal decay of the green and UV fluorescence waveforms on the buffer-gas pressure demonstrates that the two bands do not originate from a common upper state. The interdependence of the two bands, however, is clear from the disappearance of gain at 506 nm, when an optical cavity having a high Q at 342 nm is installed around the excited medium ($I_{UV} \sim 30$ MW cm^{-2}). Also, the peak intensity of the UV band is suppressed by more than 40% when a green dye-laser pulse ($\lambda \approx 503$ nm, $I \geq 5$ MW cm^{-2}) is directed along the axis of the active medium.

Gain has recently been observed[1] in molecular iodine (I_2) over a ~13-nm spectral region in the green, when mixtures of Ar and HI are pumped by a relativistic electron beam (e beam). Although this particular band had been observed in prior experiments,[2-4] the use of I_2 itself as the iodine donor in virtually all the early research precluded the realization of gain in the visible because of strong absorption by the homonuclear molecule. HI avoids that obstacle, and the observation of gain prompted a reexamination of the electronic states involved. In a previous paper,[1] it was reported that the gain coefficient at 506 nm was 1.2% cm^{-1} despite the fact that the $D' \rightarrow A'$ band was superfluorescing. Also, preliminary experimental observations indicated that the two bands were collisionally coupled (indeed, earlier workers had suggested that the two bands shared a common upper state). The results of an investigation into the degree of coupling between the UV (342-nm) and green (506-nm) bands of I_2 are described in this paper.

For the initial experiments, the apparatus was identical to that described previously,[1] except that a Tektronix 7912 AD transient digitizer recorded the emission waveforms. Briefly, a coaxial diode, 23 cm in length, ~18 cm^3 active volume, and driven by a Febetron 706 generator (3-nsec, ~600-kV pulses), provided the excitation for the gaseous medium. Research-grade Ar and electronic-grade HI were used throughout, and mixtures of the two gases were prepared in a steel cylinder. Waveforms of the axial fluorescence were obtained with a vacuum photodiode (S-20 photocathode), appropriate bandpass (342-nm band: $\lambda_0 = 350$ nm, $\Delta\lambda = 55$ nm; 506-nm band: $\lambda_0 \simeq 500$ nm, $\Delta\lambda \simeq 38$ nm) and neutral-density filters, and a Tektronix 7912 AD transient digitizer. For measurements of the gain coefficient on the green excimer band, the beam from a flashlamp-pumped, tunable dye laser (Chromatix CMX-4, linewidth $\sim 8 \times 10^{-2}$ nm, pulse width ~ 0.8 μsec) was directed along the axis of the coaxial diode, attenuated by neutral-density filters, and detected by the vacuum photodiode. The arrival of the dye-laser pulse at the gas cell could be continuously varied with respect to the initiation of the e-beam pulse by using digital-pulse and delay generators.

Representative temporal waveforms for the I_2 UV and green bands are given in Fig. 1. For a gas mixture of 0.3% HI in 5930-Torr Ar, the $D' \rightarrow A'$ band is superfluorescing, which gives rise to the narrow emission pulse. Attenuation of the UV signal by over 6 orders of magnitude was required to keep the two signal magnitudes comparable. Note that the peak UV intensity of ~2 MW cm^{-2} coincides with a noticeable decline in the green-band fluorescence. This phenomenon was extremely reproducible and is the first (indirect) indication that the two bands are coupled.

An examination of the amplitude and temporal half-width (HWHM) of the green and UV I_2 waveforms (Figs. 2 and 3, respectively) shows that not only are the transition probabilities for the two bands completely different but their temporal histories are dissimilar even at the highest buffer-gas pressures studied (~6000 Torr). In the low-pressure limit, the half-widths converge since collisional relaxation of the higher-lying ion pair states is the rate limiting process. However, as the Ar buffer-gas pressure is increased (HI concentration held constant), the fluorescence half-widths for the two emission pulses approach lower limits that differ by roughly a factor of 2 and are related to the collisionally quenched, effective lifetime for each upper electronic state. The 5-nsec half-width of the 342-nm emission pulse for large partial pressures of Ar is not due to superfluorescence, as the partial pressure of HI was intentionally reduced and held constant at 1 Torr to avoid this possibility.

More direct evidence for the upper states of the two bands being distinct but closely coupled is obtained by artificially increasing the UV flux in the medium with an optical cavity. Various intracavity intensities were obtained by using combinations of uncoated quartz flats and dielectric coated mirrors (2-m radius of curvature, $R > 99\%$ at 342 nm) to form the cavity. Thus either a flat or a mirror was placed at either end of the cylindrical diode, and the cavity was aligned with the dye-laser probe beam. By changing the cavity Q in this manner, the intracavity UV intensity could be varied from 1.8 to ~30 MW cm^{-2}. The effect of increasing the UV intensity on the gain coefficient of the green excimer band at 506 nm

0740-3224/85/030430-03$02.00

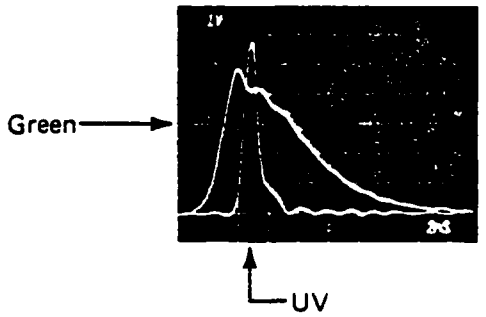

Fig. 1. Waveforms for the green ($\lambda \sim 506$ nm) and UV (342-nm) bands of I_2 that were recorded with a Tektronix 7104 oscilloscope and a Hammamatsu R1193U-03 photodiode. The temporal resolution is 2 nsec/division, and the 342-nm emission has been attenuated by 6 orders of magnitude for the sake of comparison. The gas mixture is 18-Torr HI/6000-Torr Ar. Note the depression of the green emission at the peak of the UV intensity (~2 MW cm^{-2}).

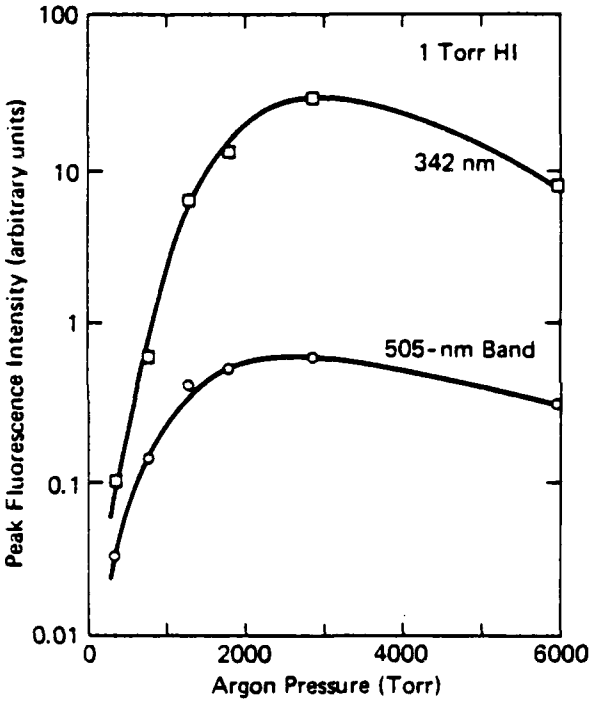

Fig. 2. Relative peak-fluorescence intensity of the UV and green bands of I_2 as a function of the Ar-buffer pressure.

is shown in Fig. 4, where the solid line is simply a smooth curve drawn through the data. In the absence of an optical cavity, the peak gain coefficient is 1.4% cm^{-1}, but for $I_{342\ nm}$ (circulating UV intensity) ~30 MW cm^{-2}, amplification in the green has vanished. The steep slope of the curve at 1.8 MW cm^{-2} supports earlier calculations,[1] which indicate that the 506-nm gain coefficient at this intensity is less than 20% of its small-signal value. Although eliminating the UV radiation entirely would be a preferable means of illustrating the deleterious effect of the $D' \rightarrow A'$ emission on the green band's gain, several attempts to do this with intracavity absorbers (glass filters, vapor additives to the gas mixture, etc.) were unsuccessful.

When an intense, *green* dye-laser pulse is injected into the active medium (optical cavity removed) using the apparatus diagramed in Fig. 5, the converse effect is observed. In order to saturate the green excimer band, several experiments were conducted with a KrF-pumped dye laser having a linewidth of 5×10^{-3} nm and a spectral range of 80 nm (470–550 nm) for Coumarin 500 dye.[5] The pulse energy (at 506 nm) was

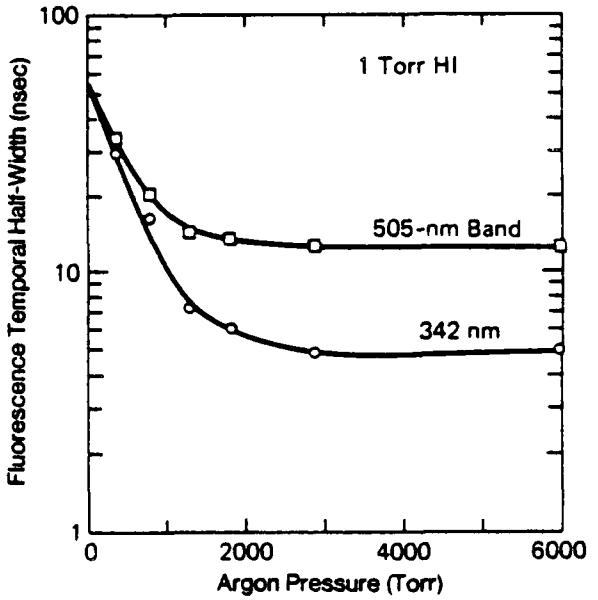

Fig. 3. Ar pressure dependence of the temporal half-width of the I_2 green- and UV-fluorescence waveforms. For all the data shown, the HI partial pressure was fixed at 1 Torr. Limiting the HI concentration was necessary to prevent superfluorescence on the I_2 $D' \rightarrow A'$ band at 342 nm.

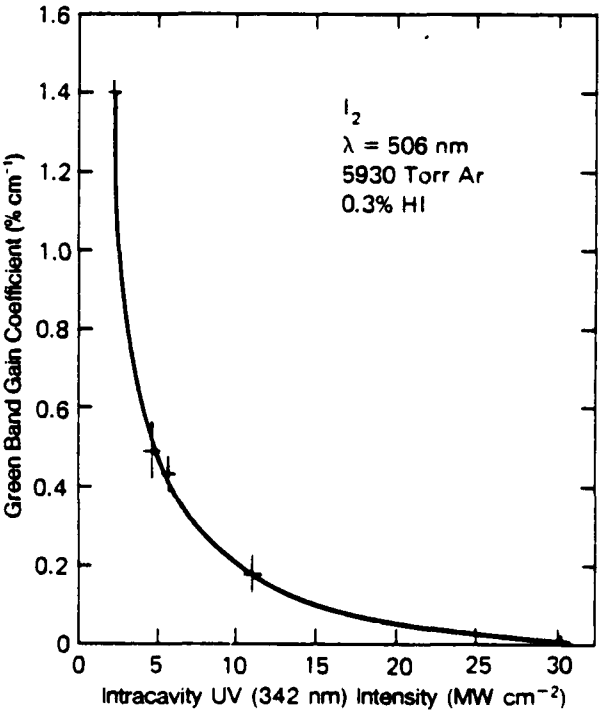

Fig. 4. Variation of the gain coefficient at 506 nm, with the UV intensity circulating in the optical cavity. Note the steep slope of the curve at the lowest UV intensity studied (1.8 MW cm^{-2}).

nominally 10 mJ, and spatial filtering of the beam with irises ensured reproducible results. In this experiment, the 20-nsec FWHM dye-laser pulse is timed to coincide with the peak in the UV emission.

As shown in Fig. 6 for a dye-laser wavelength of 503 nm, a pronounced effect is observed on the 342-nm intensity. For a green-laser-pulse intensity of ~13 MW cm^{-2}, the peak UV emission has fallen to ~35% of its initial ($I_{Green} = 0$) value. When the dye laser is tuned to a wavelength at the extremity of the green gain band (490 nm—see Fig. 4 of Ref. 1) the effect, as expected, is considerably weaker. The intensity at 490 nm that is required to suppress the integrated UV-band intensity by 25% is approximately three times greater than that necessary at 503 nm (~4 MW cm^{-2}).

A rough estimate of the collisional rate constant necessary to explain these results can be found by letting σ_{SE} (the UV-band stimulated-emission cross section) $= 5 \times 10^{-16}$ cm^2 and $\hbar\omega_{UV} = 5.8 \times 10^{-19}$ J. Therefore the stimulated-emission rate at 342 nm is $\sigma_{SE} I_{UV} (\hbar\omega)^{-1} = 1.7 \times 10^9$ sec^{-1} for an intensity of 2 MW cm^{-2} (no injected green-laser energy). Next, quenching of the I_2 D' state is ignored, and it is assumed that collisional transfer of excited I_2 molecules to the upper state for the green band is the dominant nonradiative loss mechanism for the D' level in the presence of the 503-nm optical field. Hence, defining k_1 by the two-body reaction

$$I_2^*(D') + Ar \xrightarrow{k_1} I_2^{**} + Ar, \qquad (1)$$

where I_2^{**} represents an excited molecule in the green band's upper state, then $k_1[Ar] \sim (0.8 - 1.0) \times 10^9$ sec^{-1} or $k_1 \sim 4 \times 10^{-12}$ cm^3 sec^{-1}. This value is an order of magnitude below gas kinetic and indicates that the intensities required to suppress the emission of either band are reasonable.

In summary, the competition between the UV ($D' \rightarrow A'$) and green excimer bands of I_2 has been studied by examining the effect on each of the two transitions of increasing the intensity on the other. The two bands clearly do not originate from a common I_2 electronic state (as indicated by the temporal dependence of their respective emission waveforms), but the levels in question probably lie within several KT of one another. Temperature-dependent emission measurements will be required to clarify the position of the two levels further. The ability to deplete the D' population with a strong optical field at 506 nm suggests that an efficient, continuously tunable green-laser system utilizing I_2 as the oscillator *or* amplifier is feasible.

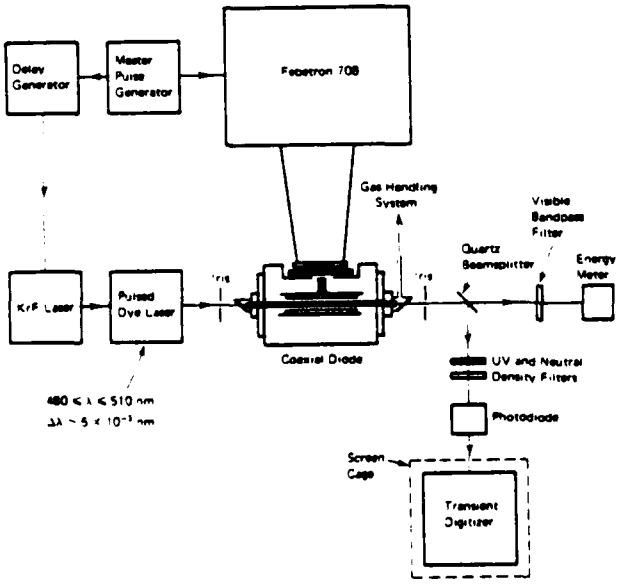

Fig. 5. Schematic diagram of the experimental apparatus used in suppressing the $I_2(D' \rightarrow A')$ UV emission.

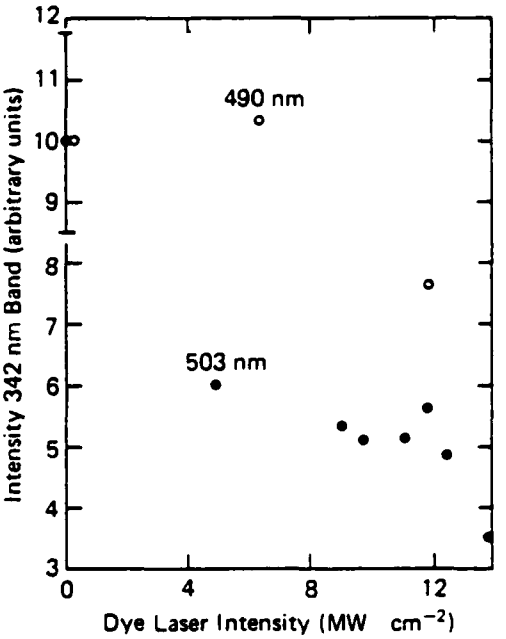

Fig. 6. Dependence of the peak UV-band intensity on the dye-laser intensity injected into the medium. At 13 MW cm^{-2} and a probing wavelength of 503 nm, the 342-nm intensity is depressed to 35% of its initial value (2 MW cm^{-2}). The ~17% uncertainty in the UV intensity for $I_{Green} = 0$ is indicated by the error bars on the vertical axis.

ACKNOWLEDGMENTS

The authors appreciate the technical assistance of B. Witt, C. Henderson, Y. Moroz, K. Flessner, and D. Watterson. This research was supported by the National Science Foundation (J. Aller) under grant ECS 83-09641 and the U.S. Army Research Office (B. Guenther) under grant DAAG 29-83-K-0108.

REFERENCES

1. K. P. Killeen and J. G. Eden, "Gain on the green (504-nm) excimer band of I_2," Appl. Phys. Lett. 43, 539–541 (1983).
2. A. L. Guy, K. S. Viswanathan, A. Sur, and J. Tellinghuisen, "Reinterpretation of the emission spectrum of I_2 in argon," Chem. Phys. Lett. 73, 582–588 (1980).
3. H. Hemmati and G. J. Collins, "Studies of the blue-green fluorescence from iodine molecules excited by a 193-nm ArF laser," Chem. Phys. Lett. 67, 5–8 (1979); "Laser excited fluorescence of I_2," Chem. Phys. Lett. 75, 488–493 (1980).
4. V. N. Baboshin, L. D. Mikheev, A. B. Pavlov, V. P. Fokanov, M. A. Khodarkovskii, and A. P. Shirokikh, "Investigation of luminescence and excitation spectra of molecular iodine," Sov. J. Quantum Electron. 11, 683–684 (1981) [Kvantovaya Electron. (Moscow) 8, 1138–1141 (1981)].
5. Exciton Chemical Company, Dayton, Ohio.

Reprinted from

Applied Physics Letters

Volume 48 5 May 1986 Number 18

$X^2\Sigma \rightarrow B^2\Sigma$ absorption band of HgBr: Optically pumped 502-nm laser

D. P. Greene,[a] K. P. Killeen,[a] and J. G. Eden
University of Illinois, Urbana, Illinois 61801

(Received 17 Oetober 1985; accepted for publication 10 March 1986)

pp. 1175-1177

a publication of the American Institute of Physics

$X^2\Sigma \rightarrow B^2\Sigma$ absorption band of HgBr: Optically pumped 502-nm laser

D. P. Greene,[a] K. P. Killeen,[a] and J. G. Eden
University of Illinois, Urbana, Illinois 61801

(Received 17 October 1985; accepted for publication 10 March 1986)

The $X\,^2\Sigma^+_{1/2} \rightarrow B\,^2\Sigma^+_{1/2}$ absorption band of HgBr has been observed in the afterglow of a pulsed Ne-N_2-$HgBr_2$ discharge. Peaking in the ultraviolet (UV) near 350 nm, this continuum degrades slowly to the red and at 410 nm the absorption coefficient is 30% of its maximum value. Upon exciting the $X \rightarrow B$ band with an XeF (351 nm) or frequency tripled Nd:YAG (355 nm) laser, intense lasing is observed in the blue-green ($\lambda \sim 502$ nm). For $\lambda_{pump} = 351$ nm, the energy conversion efficiency (UV to green) is 22% which corresponds to a *photon* conversion efficiency of 32%. The quantum efficiency for this four level system is 71%.

Below the ionically bound $B\,^2\Sigma^+_{1/2}$ excited state of HgBr lie two levels which correlate with $Hg(^1S_0) + Br(^2P_{1/2,3/2})$ in the separated atom limit. The ground state, $X\,^2\Sigma^+_{1/2}$, is bound by 0.48–0.7 eV (Refs. 1–3) while the $A\,^2\Pi_{1/2,3/2}$ curves are dissociative. Also, the Franck–Condon shift of B with respect to X is large ($R_{eB} \simeq R_{eX} + 0.6$ Å). Owing to the large dipole moment between $B(v' = 0)$ and high-lying vibrational levels ($v'' = 22,23$) of the X state, radiative decay of the $B\,^2\Sigma$ level is dominated by a highly structured emission band peaking at $\lambda \sim 502$ nm. Several groups[4,5] have studied the $B \rightarrow X$ fluorescence spectrum in detail and Lapatovich *et al.*[6] have observed the much weaker $B \rightarrow A$ continuum in the red.

Less is known of the absorption spectrum of the HgBr radical ground state. The $C,D \rightarrow X$ bands of HgBr were first observed (in emission) in 1929 (Ref. 4) but $X \rightarrow C$ absorption was not reported until much later.[7] Recently, Krauss and Stevens[1] published theoretical predictions for the $X \rightarrow A$ photodissociation spectrum in the visible ($\lambda_{max} \sim 650$ nm).

In this letter, the observation of the $X \rightarrow B$ absorption band and experiments in which the B state is pumped directly from ground by an ultraviolet (UV) laser are reported. Figure 1 shows the visible and UV gain/absorption spectrum of a pulsed HgBr laser discharge containing a mixture of Ne (3.8×10^{19} cm^{-3}), N_2 (3.2×10^{18} cm^{-3}), and $HgBr_2$ vapor (4.1×10^{16} cm^{-3}; $T = 420$ K) at a total room temperature pressure of 760 Torr. Two spectra are given, one acquired during the active discharge and one $\sim 1\ \mu$s in the afterglow. The transverse discharge device and optical detection system were similar to those described previously for studies of excited state absorption in the cadmium monoiodide radical.[8] Briefly, a pulsed xenon lamp having a temporal width of 300 ns FWHM produced a continuum which, after being spatially filtered and collimated, traversed the length of the 50 cm, UV-preionized discharge region. An optical multichannel analyzer (OMA) and a 0.25-m spectrograph (operated in first order) recorded the transmitted spectrum. This system has a relatively flat response between 200 and 950 nm and a spectral resolution of ~ 0.2 nm.

The two most prominent features in Fig. 1 are the quasi-continuum in the near UV and the structured $B \rightarrow X$ gain profile in the green. As will be discussed in detail elsewhere, the apparent "gain" between the $X \rightarrow C$ and $X \rightarrow D$ bands (centered near 285 and 255 nm, respectively) actually arises from the increased transparency of the medium in this spectral region due to depletion of the $HgBr_2$ concentration by electron impact dissociation. The $HgBr_2$ ($1\,^1\Sigma_g^+ \rightarrow 1\,^1\Pi_u$) absorption continuum lies in this region.[9–11]

Peaking near 350 nm, the $X \rightarrow B$ band of HgBr is broad (FWHM ~ 60 nm), is slightly skewed towards the red and, owing to the small vibrational frequencies of both states, is essentially a continuum. However, the obvious structure between 385 and 365 nm is real. Temporally resolved measurements of the $X \rightarrow B$ continuum show that it is most intense 80–200 ns in the afterglow and, at later times, decays with an exponential constant of $\sim 1\ \mu$s.

Because of the relatively low photon energies required to access the $B\,^2\Sigma$ state from ground (~ 3.5 eV), one can quickly envision an optically pumped HgBr ($B \rightarrow X$) laser having a high quantum efficiency (2.5 eV/3.5 eV = 71%). In subsequent experiments, therefore, a ~ 8-ns pulse from a frequency-tripled, Q-switched Nd:YAG ($\lambda = 355$ nm) or XeF (351 nm, 15-ns pulse) laser was directed along the axis of the Ne/N_2/$HgBr_2$ discharge. An optical cavity having a moderate Q at 502 nm (first mirror: $R = 99\%$ at 502 nm, 10% at 351 nm; second mirror: $R = 16\%$ at 502 nm) was installed around the discharge cell and a UV laser pulse entered the plasma after passing through the first mirror. A cylindrical lens telescope compressed the ~ 2.5 cm^2 pump beam so as to match the small cross-sectional area of the HgBr discharge (~ 0.4 cm^2). Digital delay generators allowed for the external laser pulse to arrive at any specified time Δt with respect to the peak discharge current.

Oscillograms of the HgBr ($B \rightarrow X$) laser waveforms produced as a result of this arrangement are shown in Fig. 2. A vacuum photodiode (S-20 photocathode) viewed the discharge along its axis through a 500-nm dielectric bandpass filter ($\lambda_0 \simeq 495$ nm, $\Delta\lambda = 40$ nm). In the absence of external radiation, the HgBr (B) state is excited by the discharge in the conventional way[12] and a laser pulse having a ~ 40 ns FWHM is emitted. The arrival of a 16.5 mJ, XeF (351 nm) pulse ~ 85 ns after the onset of the discharge current [Fig. 2(b)] results in the production of a second laser pulse having a FWHM roughly the same as that of the pump (16 ns).

[a] Visiting Research Associate, 1985

 0003-6951/86/181175-03$01.00

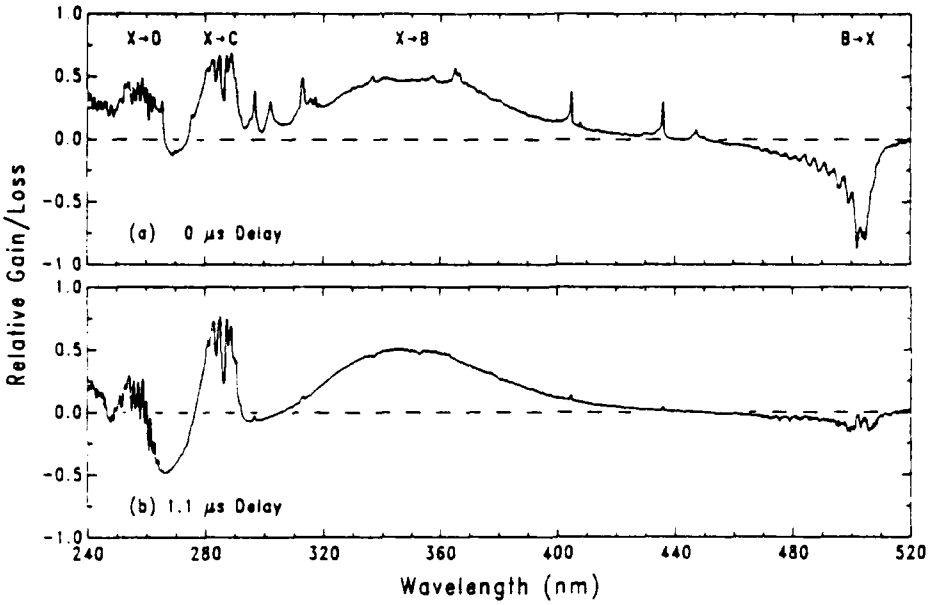

FIG. 1. Transient gain and absorption spectra of a pulsed Ne, N_2, $HgBr_2$ vapor discharge from 230 to 530 nm. Spectra were acquired: (a) when the peak Xe lamp output coincided with maximum discharge current (and HgBr fluorescence) and (b) 1.1 μs into the discharge afterglow. The dashed line indicates medium transparency. Portions of the trace above and below the dashed line normally represent absorption and optical gain (negative loss), respectively. However, the excursion of the curves in both (a) and (b) below the line between 260 and ~305 nm is *not* due to gain in that region but rather to the depletion of the $HgBr_2$ number density owing to electron impact dissociation in the discharge. $HgBr_2$ absorbs strongly in that spectral range. Also, note that the $B \rightarrow X$ band exhibits gain even at wavelengths below 470 nm.

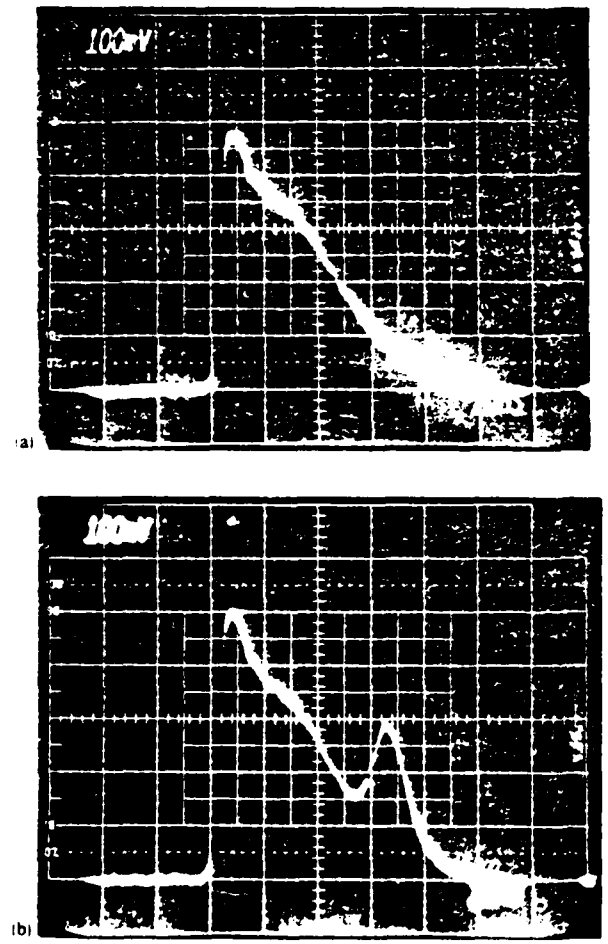

FIG. 2. HgBr laser waveforms that are observed: (a) without and (b) with a 351-nm XeF laser injected into the HgBr laser cavity. Of the 16.5 mJ in the XeF pulse, 13 mJ (79%) was absorbed by the discharge and the energy in the second HgBr pulse is 3 mJ. Thus, the energy and photon conversion efficiencies are 22.8% and 32.6%, respectively. UV to blue-green conversion efficiencies exceeding 20% were observed reproducibly. Time base is 20 ns/large division.

If the discharge is not fired, nothing is observed at the photodiode when the XeF (or Nd:YAG) radiation passes through the $HgBr_2$ vapor column. These results confirm that the 351-nm photons are directly exciting HgBr ($B\,^2\Sigma$) from $X\,^2\Sigma$ and that the discharge serves solely as a source of ground state HgBr radicals.

As shown in Fig. 3, detailed measurements of the additional 502-nm energy produced for a known value of 351-nm input energy yield a UV-to-green energy conversion efficiency of 22% or a *photon* conversion efficiency of 32%. Thus, the efficiencies that have been observed are approximately 1/3 of the theoretical maximum. No effort has yet been made to optimize the conversion efficiency through the choice of cavity output coupling. Each data point in Fig. 3 has a maximum uncertainty of $\pm$ 10%.

Note that pumping the $X \rightarrow B$ band of HgBr at $\lambda = 350$ nm populates high lying vibrational states of the $B\,^2\Sigma$ level ($v' \simeq 50$, lying ~0.5 eV above T_e but still ~2 eV below the Hg ($6\,^3P_1$) + Br separated atom limit) because of the large Franck–Condon shift between the two electronic states. Since lasing is observed only from the $v' = 0$ and 1 levels and since the *photon conversion efficiency* is large (~1/3), one concludes that, as observed by Roxlo and Mandl,[13] vibrational relaxation in the B state is both rapid and efficient. Similarly, the rate coefficients for removal of the ground state vibrational levels ($v'' = 22,23$) are known to be gas kinetic [for example, $k_Q(N_2) = 4.8 \times 10^{-10}$ cm^3 s^{-1}].[14]

Schimitschek *et al.*[15] first photo pumped the HgBr laser in 1977 by photodissociating $HgBr_2$ at 193 nm. Despite the fact that the overall quantum efficiency for this process (2.5 eV/6.4 eV ≃ 39%) is within a factor of 2 of that for the scheme reported here, maximum energy conversion efficiencies of < 5% have been reported to date. The loss of energy from the transient intermediate species $HgBr_2^*$ to nonradiative channels *other* than HgBr* (B) + Br may account for the comparatively low efficiency for the HgBr photodissociation pumped laser.[9] This conclusion is consistent with the quantum efficiency for HgBr ($B \rightarrow X$) fluorescence of 26%

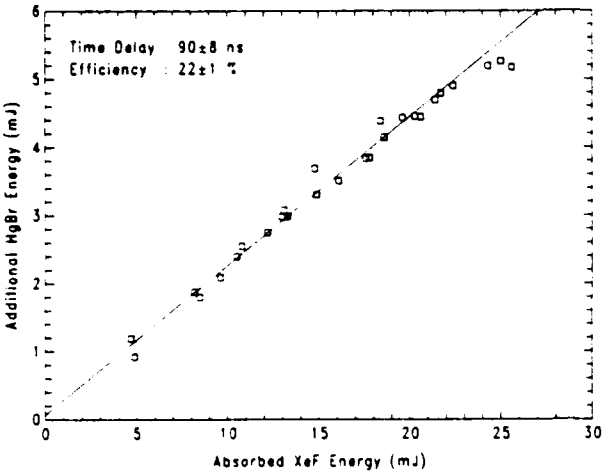

FIG. 3. Efficiency for conversion of 351-nm pump into 502-nm output energy (Δt held constant at 90 ns). The slope of the linear least-squares fit to the data (solid line) is 22%.

that was measured by Maya[16] for $HgBr_2$ vapor irradiated at 205 ± 15 nm.

In summary, the $X\,^2\Sigma \rightarrow B\,^2\Sigma$ absorption band of HgBr has been observed and, under the present experimental conditions, lasing is observed for XeF laser fluences below 0.8 MW cm^{-2}. Direct excitation of the B state from ground with an XeF or tripled Nd:YAG laser pulse results in a UV-to-blue-green conversion efficiency of 22% which roughly corresponds to the emission of one 2.5-eV photon for every three absorbed 3.5-eV photons. The breadth of the 350-nm centered absorption spectrum and the large associated absorption coefficient ($\sim 10^{-16}$ cm^2) suggest that this four level system is an excellent candidate for a flashlamp-pumped laser. One of the chief advantages of such a scheme is that, once dissociated, it is not necessary (and is, in fact, undesirable) for the $HgBr_2$ parent to reform. Thus, fuel depletion is not the potential liability that it is with the dissociation laser since, following stimulated emission of an HgBr molecule to ground, the radical is immediately available for re-excitation to the upper laser level. Also, contrary to other well-known, optically pumped diatomic lasers, laser emission in the present experiments *only occurs from vibrational levels that are not pumped*. It appears that pump radiation can be absorbed over a broad spectral range by a large number of vibrational states and funneled into one or two radiating levels.

The authors acknowledge the expert technical assistance of K. Kuehl, Y. Moroz, P. Hayes, and D. Watterson. The assistance of C. C. Abele in data acquisition and analysis is especially appreciated. This work was supported by the National Science Foundation (J. Aller) under grant ECS 83-09641 and the Army Research Office (B. Guenther) under contract DAAG 29-83-K-0108.

[1] M. Krauss and W. J. Stevens, Appl. Phys. Lett. **39**, 686 (1981).
[2] W. R. Wadt, Appl. Phys. Lett. **34**, 659 (1979).
[3] R. E. Wilcomb and R. B. Bernstein, J. Mol. Spectrosc. **62**, 442 (1976).
[4] K. Wieland, Helv. Phys. Acta **2**, 46 (1929).
[5] J. Tellinghuisen, in *Excimer Lasers-1983*, edited by C. K. Rhodes, H. Egger, and H. Pummer (AIP, New York, 1983), pp. 99–105.
[6] W. P. Lapatovich, G. R. Gibbs, and J. M. Proud, Appl. Phys. Lett. **41**, 786 (1982).
[7] K. Wieland, Helv. Phys. Acta **19**, 408 (1946).
[8] D. P. Greene and J. G. Eden, Opt. Commun. **53**, 263 (1985); J. Chem. Phys. **82**, 702 (1985).
[9] W. R. Wadt, J. Chem. Phys. **72**, 2469 (1980).
[10] C. Roxlo and A. Mandl, J. Appl. Phys. **51**, 2969 (1980).
[11] D. Spence, R. G. Wang, and M. A. Dillon, Appl. Phys. Lett. **41**, 1021 (1982).
[12] That is, by excitation transfer from N_2 (A) to dissociate $HgBr_2$ and produce the HgBr (B) state; see E. J. Schimitschek and J. E. Celto, Opt. Lett. **2**, 64 (1978); R. Burnham, Appl. Phys. Lett. **33**, 156 (1978); E. J. Schimitschek and J. E. Celto, Appl. Phys. Lett. **36**, 176 (1980).
[13] C. Roxlo and A. Mandl, J. Chem. Phys. **72**, 541 (1980).
[14] H. Helvajian, M. Mangir, and C. Wittig, Chem. Phys. Lett. **71**, 177 (1980).
[15] E. J. Schimitschek, J. E. Celto, and J. A. Trias, Appl. Phys. Lett. **31**, 608 (1977).
[16] J. Maya, IEEE J. Quantum Electron. **QE-15**, 579 (1979).

Reprinted from

THE JOURNAL
OF
CHEMICAL PHYSICS

VOLUME 82 NUMBER 2

15 JANUARY 1985

Origin of the 454 nm bound→free absorption band of cadmium monoiodide (^{114}CdI)

D. P. Greene and J. G. Eden
University of Illinois, Urbana, Illinois 61801

pp. 702-708

Published by the
AMERICAN INSTITUTE OF PHYSICS

Origin of the 454 nm bound→free absorption band of cadmium monoiodide (^{114}CdI)

D. P. Greene and J. G. Eden
University of Illinois, Urbana, Illinois 61801

(Received 6 September 1984; accepted 11 October 1984)

The bound→free absorption band recently observed in a ^{114}CdI laser discharge [Greene and Eden, Opt. Comm. (1985)] is shown to arise from absorption by the $B\,^2\Sigma$ excited state of ^{114}CdI to a previously unobserved level lying $\sim 4.3\times10^4$ cm^{-1} above ground. Pumping of the absorptive transition with a pulsed blue dye laser strongly suppresses gain (and, hence, laser output power) on the $B\rightarrow X$ band in the red (657 nm). Therefore, this constitutes the first known report of an ionic excited state→covalent absorption band [i.e., $(M^+X^-)+\hbar\omega\rightarrow M^*+X$; M, X = metal and halogen atoms, respectively] for any of the group IIB metal halides *or* rare gas–halide laser molecules. Also, ω_e for the $B\,^2\Sigma$ state of ^{114}CdI is $\gtrsim 110$ cm^{-1} (considerably larger than an existing value in the literature) and the terminal level for this blue absorption band is tentatively assigned to a dissociative $^2\Sigma$ state correlated with the Cd($5p\,^3P_J$) + I separated atom limit.

I. INTRODUCTION

The lowest-lying excited states of the group II B metal–halide diatomic molecules are ionic in character (M^+–X^-; M and X are group II B metal (Hg, Cd, Zn) and halogen atoms, respectively). Several electronvolts higher lie covalent molecular levels that correlate with an excited metal atom (i.e., M^*+X). A similar situation exists with the rare gas–halide molecules and shortly after the discovery of these lasers, it was recognized[1] that absorption from the lowest-lying ionic state ($B\,^2\Sigma$) to highly excited covalent states constituted a potentially serious loss mechanism. Figure 1 is a generalized energy level diagram for a II B metal–halide molecule[1] but could just as well also represent a rare gas–halide diatomic except that the ground states of the latter are much less strongly bound than is indicated by the figure.

It should be emphasized that excited state absorption by any of the rare gas–halides or group II B metal–halides has not been observed previously. This paper reports the first such observation in the metal–halides, and cadmium monoiodide (^{114}CdI), in particular. In recent experiments examining the transient absorption in a ^{114}CdI laser discharge,[2] a broad absorption band peaking near 454 nm and exhibiting distinct undulatory structure was observed. Several experiments conducted since that time and described here lead one to the conclusion that the absorber is the $B\,^2\Sigma$ species itself (upper laser level) and that the terminal level is a dissociative portion of a potential curve that correlates with the ^3P excited state manifold of cadmium and a ground state iodine atom.

II. 454 nm ABSORPTION BAND: TEMPORAL HISTORY

Panoramic and expanded views of the 454 nm absorption band that was observed in a UV - preionized discharge of 50 cm active length and containing 1.6×10^{19} cm^{-3} He, 8×10^{18} cm^{-3} N_2 and 2.7×10^{16} cm^{-3} of $^{114}CdI_2$ vapor at $T = 710$ °K (after Fig. 2 of Ref. 2) are shown in parts (a) and (b), respectively, of Fig. 2. While the band peak and at least three undulations to the red are clearly visible, some structure is obscured by the two Cd atomic absorption lines. However, it should be noted that the energy separation between the undulation at ~ 462 nm and the next discernible one at 472 nm is ~ 588 cm^{-1} = 3 (196 cm^{-1}) and 192 cm^{-1} is the average spacing between the other local maxima in the spectrum.

Figure 3 is a schematic diagram of the apparatus used to determine the temporal history of the blue absorption. Individual lines from an Ar^+ ion laser traversed the $1.7\times0.15\times50$ cm^3 discharge along its axis and the transmitted beam was dispersed by a 0.5 m monochromator and detected by a photomultiplier. The oscilloscope was triggered by the leading edge of the signal from the ^{114}CdI discharge $\dot{B}$ current monitor.

Photographs of the absorption waveform for $\lambda = 457.9$ and 514.5 nm are given in Fig. 4. The discharge current (increasing downwards) accompanies each absorption waveform and, in each photograph, both waveforms share a common baseline. For the middle photograph, the probe wavelength is 457.9 nm which lies near the peak of the first undulation in Fig. 2. At this wavelength, the appearance of absorption coincides with the onset of discharge current and

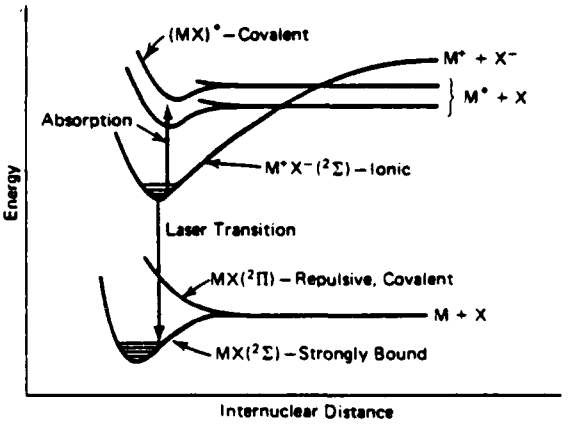

FIG. 1. Generalized energy level diagram for the group II B metal–halide molecules adapted from Ref. 1. A nearly identical one could be drawn for the rare gas–halide excimers.

 0021-9606/85/020702-07$02.10

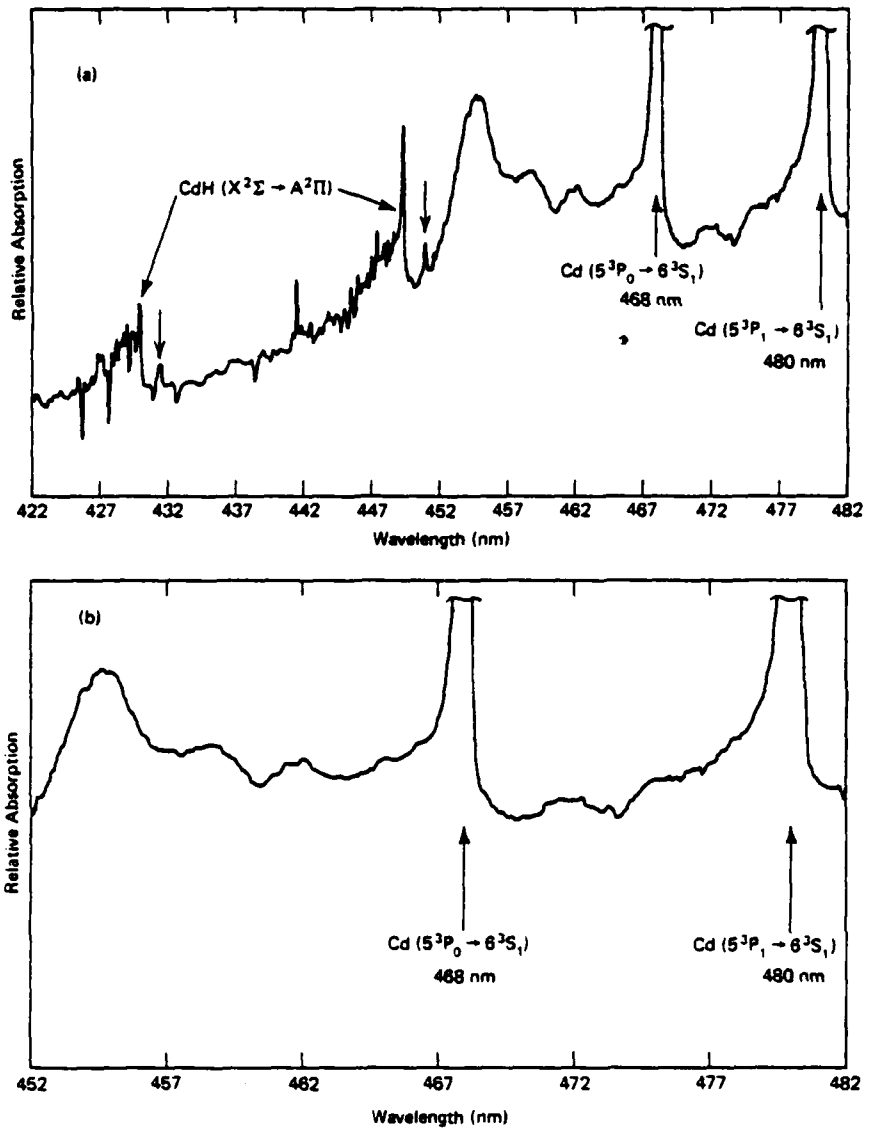

FIG. 2. Transient absorption spectrum of a $He/N_2/^{114}CdI_2$ (^{114}CdI laser) discharge (T = 710 K) in the blue showing a bound → free absorption band peaking near 454 nm. The periodicity of the undulations is (192 ± 14) cm. An expanded view of the diffuse spectrum in the blue is shown in (b).

both waveforms reach maximum in ~ 100 ns. As demonstrated by the results at 514.5 nm, the slow decay of the 457.9 nm waveform is due to optical distortion of the medium by the pulsed discharge. The green line at 514.5 nm lies well outside the blue band of interest here and the transient "absorption" recorded at this wavelength was observed at all the wavelengths studied. Therefore, if one subtracts the waveform in the top photograph from that observed at 457.9 nm, the result perfectly reproduces the temporal history of the $B \rightarrow X$ fluorescence in the red (bottom photo).

Figure 5 presents the dependence of the peak blue absorption coefficient on wavelength and $^{114}CdI_2$ partial pressure in the discharge. The dashed curve in the figure shows the rough outline of the 454 nm band and it is clear that the coefficients measured at five of the Ar^+ laser wavelengths are consistent with the band contour. Also, the temperature dependent data clearly illustrate that this band is associated primarily with the $^{114}CdI_2$ vapor and not the diluent gases He and N_2. In particular, these data are remarkably similar to those showing the dependence of the small signal gain coefficient on oven temperature.[4] Below ~ 610 K, this band is not observable and one concludes from initial appearances that the band arises from the CdI molecule itself.

On the basis of temporal history alone, however, it is unlikely that the 454 nm band shown in Fig. 2 can be associated with the $X^2\Sigma$ (ground)→$A^2\Pi$ transition of the

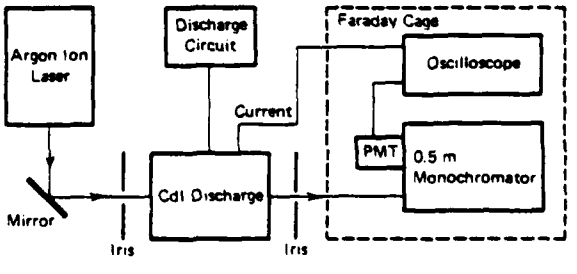

FIG. 3. Block diagram of the experimental setup for examining the temporal history of the 454 nm band.

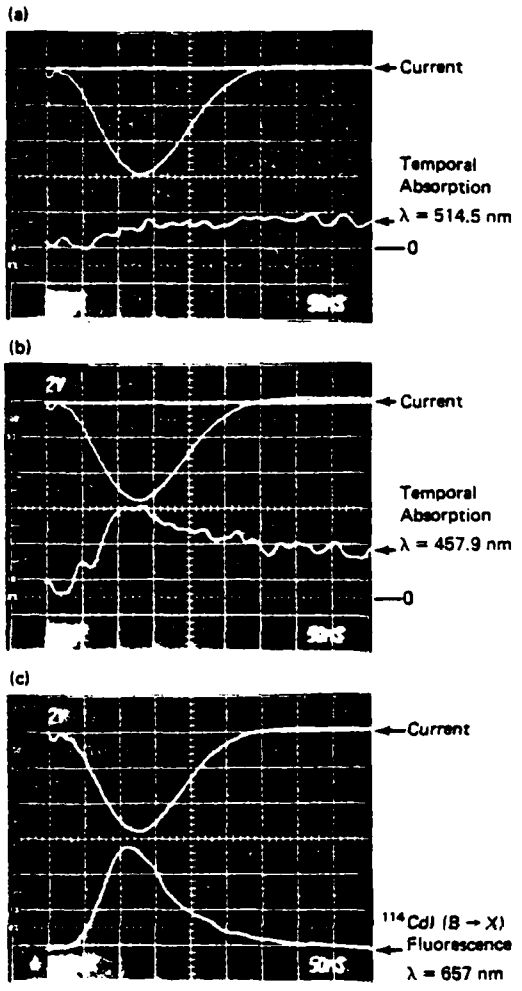

FIG. 4. Discharge current (top waveform in each photograph) and absorption waveforms observed when the CdI laser discharge was probed at two separate wavelengths. Current increases downward and the vertical sensitivity is 0.9 kA/large division. The slowly-rising signal at 514.5 nm (top) arises from an optical distortion of the medium due to the discharge. The result of probing the medium of 457.9 nm is shown in the middle photograph. Absorption increases upward. For the sake of comparison, the CdI($B \rightarrow X$) fluorescence waveform is shown in the bottom photograph.

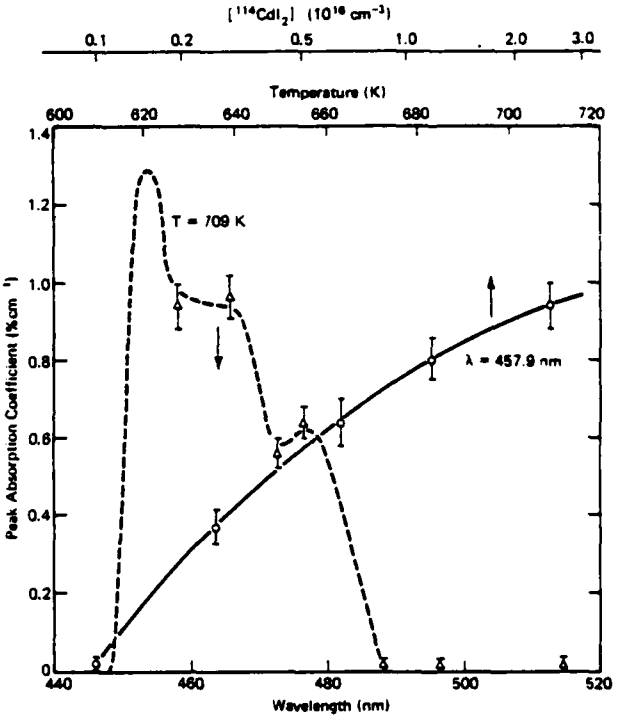

FIG. 5. Comparison of Ar^+ ion laser absorption measurements in the blue (△) with the approximate profile of the absorption band (dashed line). Also shown is the dependence of the absorption coefficient at 457.9 nm on the partial pressure of $^{114}CdI_2$ in the discharge. For all of the data shown, the He and N_2 number densities were fixed at 1.6×10^{19} cm^{-3} and 8×10^{18} cm^{-3}, respectively. The error bars reflect the uncertainty in the absorption coefficient owing to shot-to-shot variations in the power loading of the medium.

^{114}CdI molecule. As pointed out by Krauss and Stevens for HgBr (Ref. 3), the $X\,^2\Sigma$ state population is expected to monotonically increase throughout the current (pumping) pulse, leading to maximum $X \rightarrow A$ absorption well after the peak in the B state population.

III. COUPLING OF BLUE ABSORPTION AND RED $B \rightarrow X$ BANDS: SUPPRESSION OF GAIN AT 657 nm

The similarity between the ^{114}CdI ($B \rightarrow X$) fluorescence in the red and the temporal history of the blue absorption leads to the suspicion that the transient absorber in question is the upper laser level for the ^{114}CdI laser, the $B\,^2\Sigma$ state. If this is indeed the case, then exciting the blue absorption band with a saturating dye laser pulse will be accompanied by suppression of gain on the $B \rightarrow X$ band and, of course, a corresponding decline in laser output power. The near-threshold operation of the ^{114}CdI discharge laser (due primarily to the low small signal gain coefficient: 2% - cm^{-1} peak at 657 nm) increases the likelihood that even if the B state population is only slightly diminished by the 454 nm laser pulses, the output power will change substantially.

Figure 6 is a partial schematic diagram of the experimental apparatus designed to investigate the nature of the coupling (if any) between the 454 nm absorption band and the $B \rightarrow X$ laser transition. An excimer-pumped dye laser, tuned to 454 nm (peak of the absorption band in Fig. 2), produced ~ 2 mJ pulses of ~10 ns width (FWHM) from coumarin 450. These pulses were injected into the ^{114}CdI laser cavity through a 3 m radius of curvature dichroic mirror (T = 0.18% at 657 nm, 92% at 454 nm). A flat dielectric mirror and a 650 nm interference filter (T_{max} = 60%, $\Delta\lambda$ = 20 nm) blocked the transmitted blue radiation and the red laser output was detected by a vacuum photodiode. The 454 and 657 nm laser waveforms were added in the vertical amplifier on one channel of a storage oscilloscope and the sum was displayed along with the discharge current. Neutral density filters made it convenient to vary the blue laser intensity injected into the CdI discharge.

Laser and current waveforms for three values of 454 nm intensity—400, 40, and 4 kW cm^{-2}—are presented in Fig. 7. In each case, the blue laser pulse is injected into the optical cavity 85 to ~ 130 ns prior to the maximum in the red laser output pulse. The correlation between increasing blue laser intensity and a dramatic decrease in the CdI output power is obvious and was consistently observed. The strength of this

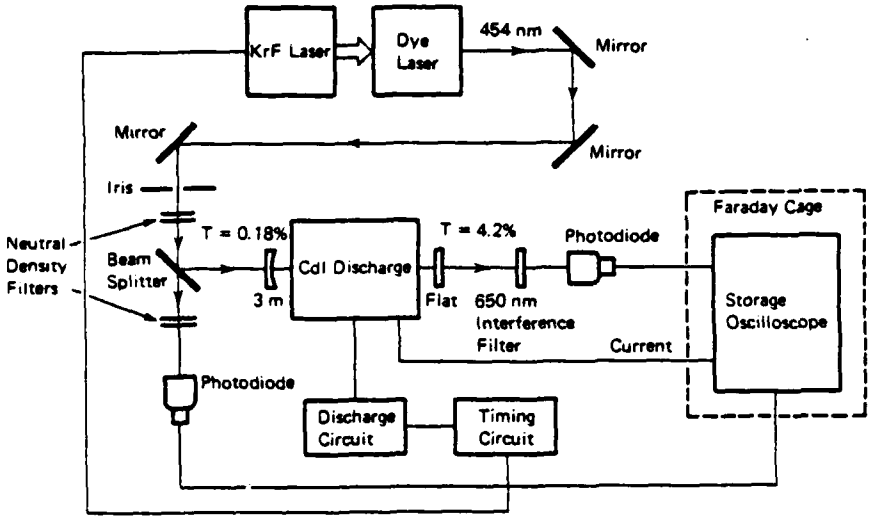

FIG. 6. Experimental apparatus for examining the effect of a blue dye laser pulse on the red output of the ^{114}CdI discharge laser. The mirror transmissions shown are those for λ = 657 nm.

effect is somewhat surprising considering that the dye laser beam cross-sectional area is only ~ 25% of the total discharge cross-sectional area but is roughly equal to the area that is lasing. Figure 8 summarizes the data that were acquired for different time delays (Δt) between the arrival of the 454 nm radiation and the onset of discharge current. The dashed horizontal line indicates the average normal (relative) output of the ^{114}CdI laser in the absence of the 454 nm radiation. Clearly, the optimal time delay is ~ 50–70 ns which places the blue laser pulse at roughly the point at which the discharge current (and, therefore, the CdI (B) excited state production rate and $B \rightarrow X$ small signal gain) is maximum. Note also that blue laser intensities < 4 kW cm^{-2} have no noticeable effect on the red laser. The 454 nm intensity required to suppress the CdI laser pulse intensity by 50% (~ 70 kW cm^{-2}) is consistent with the (125 ± 60) kW cm^{-2} saturation intensity for the CdI ($B \rightarrow X$) band that was measured recently.[5] The right-hand portion of Fig. 8 shows the dependence of the suppression of the red laser peak intensity for the three values of I and the time delay fixed at 70 ns.

Although the data of Figs. 7 and 8 indirectly support the proposed identity of the blue absorption band, these results could also be interpreted as suggesting that the 454 nm pulse is simply removing a precursor to the CdI(B) state, thus also explaining the optimal delay time of ~ 50 ns. That is, absorption of a blue (2.7 eV) photon by *either* a CdI molecule in the $B\,^2\Sigma$ state *or* by a precursor to the excited species could explain the data presented to this point and so the evidence must be considered inconclusive. More convincing support can be obtained by directly observing the $B \rightarrow X$ gain in the discharge. As illustrated in Figure 9, these final experiments involved removing the CdI laser optical cavity and counter-propagating along the discharge axis a ~0.8 μs long (FWHM) pulse from a flashlamp-pumped dye laser (Chromatix CMX-4) and the blue dye laser beam.

Oscilloscope traces of the ^{114}CdI ($B \rightarrow X$) gain at 657 nm recorded with and without the blue dye laser pulse are presented in Fig. 10. The baseline (i.e., no dye laser probe) is the horizontal line near the bottom of either photograph. The top waveform in the figure is the $B \rightarrow X$ gain waveform in the absence of the 454 nm pulse. Gain persists for ~ 60 ns (FWHM) and the waveform closely resembles the fluorescence signal shown at the bottom of Fig. 4. In the bottom photograph, the effect of an 800 kW cm^{-2} blue laser pulse on the red gain is shown. It is apparent that the B → X gain is suppressed immediately following the arrival of the 454 nm pulse. The ~ 10 ns delay between the peak of the blue laser pulse and the onset of the decline in the gain is not real but is due to the electrical arrangement of the experiment. The drawing shown in Fig. 11 is a superposition of the two gain waveforms and illustrates the gradual recovery of the $B \rightarrow X$ gain such that ~ 20 ns following the termination of the 454 nm pulse, the gain has regained its normal (unperturbed) value. Similar effects are observed regardless of the point in the $B \rightarrow X$ gain waveform at which the blue laser is fired.

One concludes, therefore, that the 454 nm centered absorption band of Fig. 2 (Ref. 2) results in the direct (immediate) depletion of the B $^2\Sigma$ state of ^{114}CdI and therefore represents a bound → free excited state absorption band of the molecule.

IV. ELECTRONIC STRUCTURE OF CADMIUM MONOIODIDE

A semiquantitative potential energy level diagram that was drawn for CdI and CdI_2 from data available in the literature is presented in Fig. 12. The energy scales on the right- and left-hand ordinates of the graph are referenced to the ground states of CdI_2 and CdI, respectively. Considering CdI_2 first, the molecule is bound by 2.5 eV (Ref. 8) and the equilibrium radius R_e for the ground state (2.63 Å) is nearly identical to that for HgI_2 (Ref. 9).

A. X, C, D and E states

For the $X\,^2\Sigma$ state of the diatomic, the dissociation energy is ~ 1.4 eV (Ref. 10) and R_e is assumed to be 2.8 Å, the same value as that for HgI (Ref. 11). Consequently, the *shape* of the CdI ground state potential is also assumed to be similar to those calculated[12,13] for several of the mercury–ha-

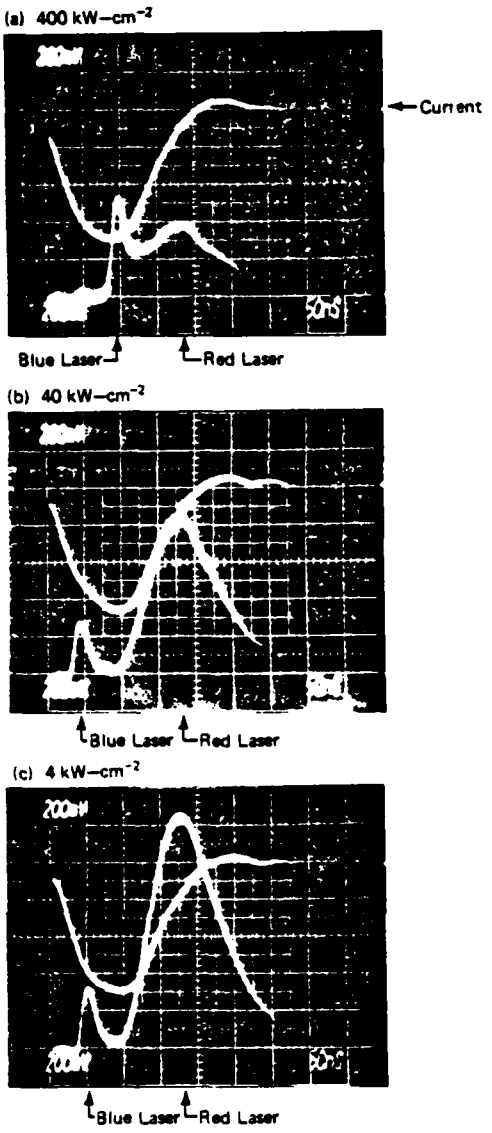

FIG. 7. Injected blue laser and ^{114}CdI ($B \rightarrow X$) 657 nm laser waveforms for $I_{454\,nm}$ = 400 kW cm^{-2} (top), 40 kW cm^{-2} (middle), and 4 kW cm^{-2} (bottom). The time base is 50 ns/large division and the current increases downward with a vertical sensitivity of 1.1 kA/large division. Also, the blue laser pulse was injected into the discharge ~85 to 130 ns prior to the peak in the 657 nm laser pulse.

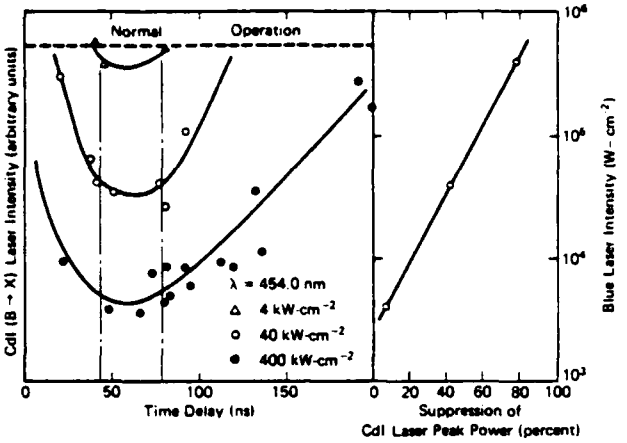

FIG. 8. Variation of the red ^{114}CdI laser output intensity with the intensity and timing of the 454 nm dye laser pulse. The dashed line indicates the intensity normally obtained from the ^{114}CdI laser in the absence of the blue radiation. The drawing to the right shows the percentage suppression of the peak 657 nm laser power for the three values of $I_{454\,nm}$ and Δt fixed at 70 ns.

lides, in which for $R > R_e$ the potential curve rapidly approaches the dissociation limit, having nearly reached the separated atom limit ~ 1.5 Å beyond R_e. Vibrational analyses of the C, D and $E \rightarrow X$ bands of CdI in the ultraviolet (~240–358 nm) show that ω_e for the $X\,^2\Sigma$ (ground) state is 179 cm^{-1}. Similarly, the vibrational constants for the $C\,^2\Pi_{1/2}$, $D\,^2\Pi_{3/2}$ and E states of CdI have been determined to be 190, 197 and 108 cm^{-1}, respectively.[14–16] The strongest lines in the $C \rightarrow X$ and $D \rightarrow X$ bands have been assigned to $v' = 0 \rightarrow v'' = 0$ transitions,[17] indicating that R_e varies little among the X, C, and D states. From the spectral positions of the $C \rightarrow X$ and $D \rightarrow X$ emission bands (10 to 30 nm to the red side of the Cd $^3P_1 \rightarrow {}^1S_0$ resonance line at 326.1 nm), it is likely that the $C\,^2\Pi$ and $D\,^2\Pi$ molecular states correlate with the $5p\,^3P$ excited states of Cd and a ground state iodine atom. In a similar vein, it is reasonable to associate the E state of CdI with the Cd ($^1P_1$) level which gives rise to the resonance line at 228.8 nm. The relative intensities of the various $E \rightarrow X$ vibrational transitions[17] indicate that the E state potential curve is only slightly shifted to larger internuclear radii with respect to the ground state.

B. $B\,^2\Sigma$ state

The $B \rightarrow X$ band of CdI has not yet been thoroughly analyzed and so the position of the B state is somewhat uncertain. Patel *et al.*[6] have interpreted a portion of the CdI emission spectrum in the blue and reported that ω_e ($X\,^2\Sigma$) = 178 cm^{-1} which is very close to the value mentioned earlier that was measured by other groups from an examination of the molecule's UV spectrum.

However, the value for the B state vibrational frequency (ω_e) reported in Ref. 6 (74 cm^{-1}) is suspiciously low for several reasons. First of all, ω_e for the B state of HgI is ~ 111 cm^{-1} (Ref. 11) and one would expect the CdI constant to be similar in magnitude. Also, it should be noted that the undulations on the blue side of the CdI ($B \rightarrow X$) fluorescence spectrum (Fig. 4 of Ref. 7) have an average periodicity $\Delta\nu$ of 109

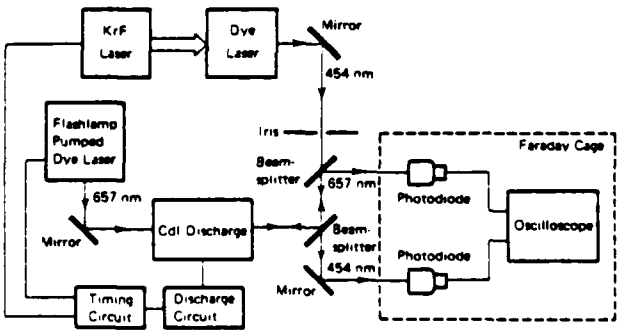

FIG. 9. Schematic diagram of the apparatus for measuring the ^{114}CdI ($B \rightarrow X$) gain in the presence of the 454 nm dye laser pulse. The two dye laser pulses were counterpropagated along the discharge axis.

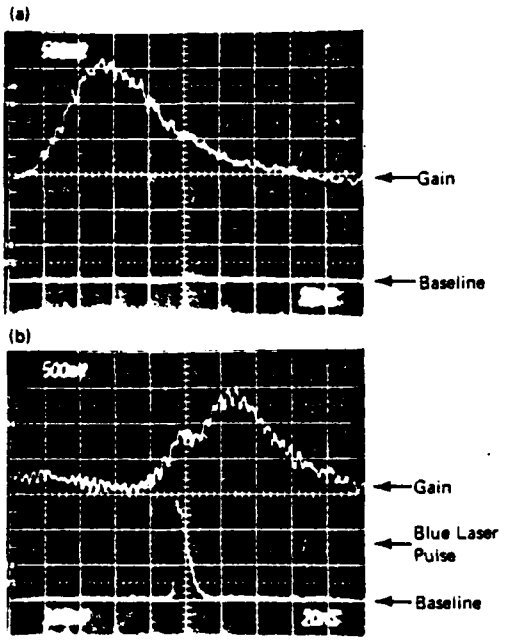

FIG. 10. Oscillograms of the gain on the $B \rightarrow X$ band of ^{114}CdI in the absence (top) and presence (bottom) of the dye laser pulse at 454 nm. The time base is 20 ns/large division.

$\pm$ 10 cm^{-1} where the error is one standard deviation in the data. Furthermore, as mentioned previously, the undulations on the red side of the 454 nm peak in the blue absorption band (Figure 2) have an average periodicity of 192 $\pm$ 14 cm^{-1}. Therefore, while Tellinghuisen and co-workers[18] have pointed out the dangers in attempting to correlate ω_e with the frequency separations between undulations in the emission spectra of the rare gas–halides, I_2 and CsXe, the following conclusions appear to be justified:

(1) ω_e for the $B\,^2\Sigma$ level is $\sim$ 110 cm^{-1} (rather than 74 cm^{-1}), in excellent agreement with ω_e for the B state of HgI,

(2) the small "vibrational spacing" mentioned in Ref. 6 reflects the fact that they are viewing high-lying vibrational levels within the B state manifold.

Verification of (1) will require higher resolution studies of both the emission and absorption spectra for the B state. The latter statement is reasonable since the spectra of Ref. 6 were acquired using an RF excited discharge *without buffer gas*. Therefore, the B state vibrational manifold is undoubtedly not equilibrated and high-lying vibrational states would be expected to be observable and perhaps dominate the spectrum.[19] The CdI discharge experiments, on the other hand, typically involve buffer gas number densities on the order of $(1\text{–}2)\times 10^{19}$ cm^{-3} and emission in the blue is extremely weak.

As far as the position of the $B\,^2\Sigma$ potential well is concerned, the drawing of Fig. 12 assumes that, in keeping with the mercury–halides, $R_e \sim 3.3$ Å. Therefore, T_e for the B state should be $\sim$ 1.2 eV above the Cd ($^1S_0$) + I ($^2P_{3/2}$) separated atom limit or $\sim$ 2.6 eV above the bottom of the X state well. Also, the B state is a long range, ionic (Coulombic) potential and thus approaches the $Cd^+ - I^-$ limit at 5.9 eV [above the Cd ($^1S_0$) + I ($^2P_{3/2}$) separated atom limit].

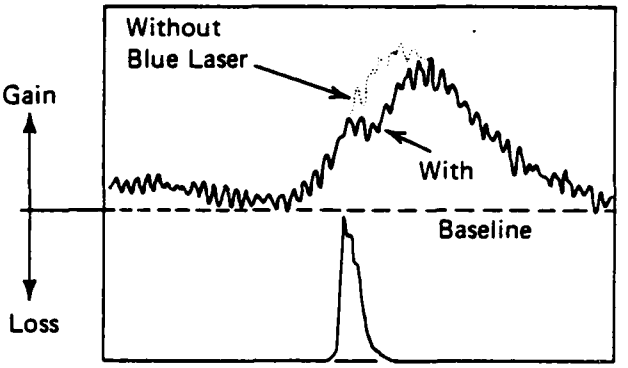

FIG. 11. Drawing of the superposition of the two gain waveforms given in Fig. 10. The suppression of the CdI ($B \rightarrow X$) gain immediately following the arrival of the blue laser pulse is obvious.

The resulting binding energy of CdI (B), $\sim$ 4.7 eV, compares favorably with the values of 4.95, 4.85 and 4.75 eV measured previously for HgCl, HgBr and HgI, respectively.[11,20]

The $A\,^2\Pi_{1/2}$ and $A\,^2\Pi_{3/2}$ states are repulsive and, in order to avoid predissociation of the B state, the $A\,^2\Pi_{3/2}$ level has been drawn such that it does not intersect the $B\,^2\Sigma$ state. Bound $\rightarrow$ free emission on the $B \rightarrow A$ band of HgBr has been reported previously.[13]

C. Identity of the 454 nm band terminal level

The experiments described earlier involved only one dye laser wavelength in the blue (454 nm) and monitoring the red CdI ($B \rightarrow X$) band at only one wavelength (657 nm). Therefore, no effort has yet been made to examine the degree of V-T relaxation within the B state manifold. However, it can be said that the near instantaneous suppression of the 657 nm gain coefficient shows that at least the population of the $B\,^2\Sigma, v' = 0$ state is being drained by the absorptive transition. From the $v' = 0$ level, a 454 nm photon ($\hbar\omega$ = 2.73 eV) has sufficient energy to reach a point just above the Cd(^3P) + I ($^2P_{3/2}$) separated atom limit. It is likely, therefore, that the terminal level for the blue CdI absorption band is a dissociative state correlating with this limit which is precisely the situation envisioned by Brau for the rare gas–halides.[1]

The $5p\,^3P$ states of cadmium and the $^2P_{3/2}$ level of iodine together give rise to six doublet states and 12 quartet levels. Ignoring $\Sigma \rightarrow \Delta$ and doublet$\rightarrow$ quartet transitions and noting that the known C and D states are probably the two $^2\Pi$ levels correlating with Cd(^3P) + I, then one is forced to the conclusion that the symmetry for the upper state of the 454 nm band is $^2\Sigma$. A qualititative profile for this state and its interaction with the bound E level are shown in Fig. 12.

Given this tentative identification of the CdI bound $\rightarrow$ free absorption band in the blue, it is now feasible to predict the peak wavelengths at which analogous transitions in several of the mercury monohalides might be observed. For HgCl, this band should appear near 345, 410, or 443 nm, depending on whether the upper state correlates with the $^3P_2$, $^3P_1$, or $^3P_0$ states of Hg, respectively. For HgBr and

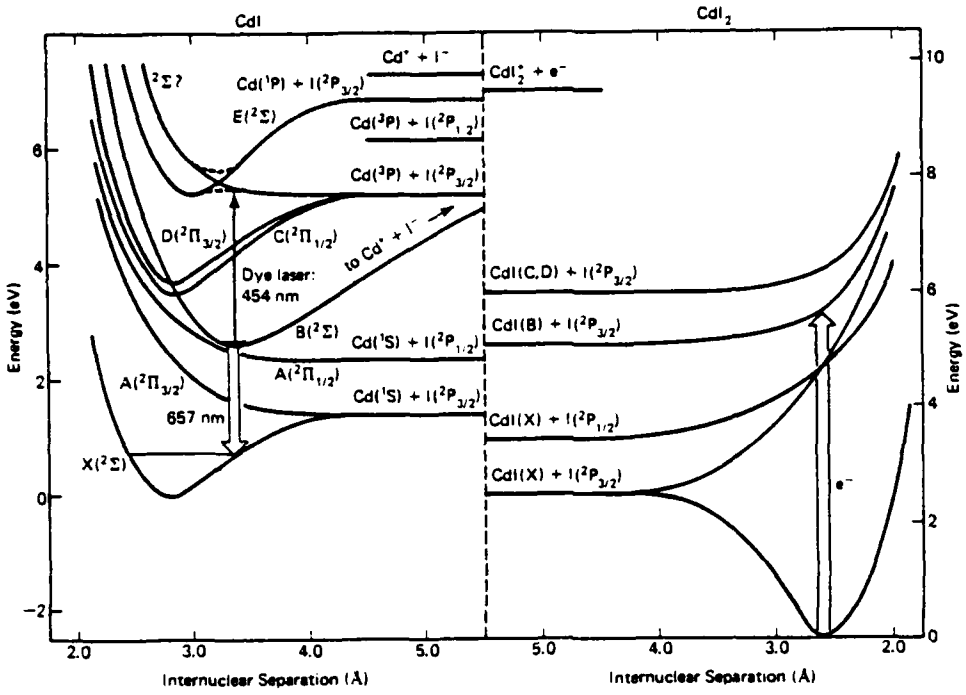

FIG. 12. Partial energy level diagram for CdI and CdI_2 showing the $B \rightarrow X$ laser band of CdI as well as excited state absorption from the $B\,^2\Sigma$ level to a state lying 2.7 eV higher in energy and associated with the limit $Cd^*(5p\,^3P_1) + I(^2P_{3/2})$.

HgI, the estimated wavelengths are 383, 464, and 506 nm and 437, 546, and 605 nm, respectively. Note that the two longest wavelengths quoted for HgBr are potential sources of interference with the $B \rightarrow X$ laser band.

V. SUMMARY AND CONCLUSIONS

The previously reported bound → free absorption band of CdI has been identified as arising from absorption by the $B\,^2\Sigma$ state (upper level for the CdI 657 nm laser) to a $^2\Sigma$ level lying 2.7 eV higher in energy. This constitutes the first known observation of excited state absorption in the rare gas–halides or group II B metal–halides. A large dipole moment is associated with this transition since it involves the transfer of an electron from the halogen to the metal atom. That is:

$$(M^+\ X^-) + \hbar\omega \rightarrow M^* + X$$

where M and X are a group II B metal atom and a halogen atom, respectively. Additional measurements, similar to those reported here, on the corresponding bands in the mercury–halides (or, perhaps, the rare gas halide species as well) will provide additional information on the structure of and kinetics within the ion-pair $B\,^2\Sigma$ state as well as more clues to the identity of the upper state.

ACKNOWLEDGMENTS

The authors are grateful to K. Kuehl, S. Piette, Y. Moroz, K. Ayers, M. N. Ediger, and K. Killeen for excellent technical assistance. This work was supported by the National Science Foundation (J. Aller) under grant ECS 83-09641 and the Army Research Office (B. Guenther) under Grant DAAG 29-83-K-0108.

[1] C. A. Brau in *Excimer Lasers*, 2nd ed., edited by C. K. Rhodes (Springer, Berlin, 1984), pp. 88 and 96; see also M. Krauss and F. H. Mies, p. 16.
[2] D. P. Greene and J. G. Eden, Opt. Comm. (to be published).
[3] M. Krauss and W. J. Stevens, Appl. Phys. Lett. 39, 686 (1981).
[4] D. P. Greene and J. G. Eden, Appl. Phys. Lett. 42, 22 (1983).
[5] D. P. Greene and J. G. Eden, Opt. Lett. (to be published).
[6] M. M. Patel, S. P. Patel and A. B. Darji, Ind. J. Pure Appl. Phys. 6, 342 (1968).
[7] D. P. Greene and J. G. Eden, Appl. Phys. Lett. 43, 418 (1983).
[8] M. Kawasaki, S. J. Lee and R. Bersohn, J. Chem. Phys. 71, 1235 (1979).
[9] D. P. Stevenson, J. Chem. Phys. 8, 898 (1940).
[10] G. Herzberg, *Spectra of Diatomic Molecules* (Van Nostrand Reinhold, New York, 1950), p. 517.
[11] J. Tellinghuisen, P. C. Tellinghuisen, S. A. Davies, P. Berwanger, and K. S. Viswanathan, Appl. Phys. Lett. 41, 789 (1982).
[12] W. R. Wadt, Appl. Phys. Lett. 34, 658 (1979).
[13] W. P. Lapatovich, G. R. Gibbs, and J. M. Proud, Appl. Phys. Lett. 41, 786 (1982).
[14] C. Ramasastry and K. R. Rao, Ind. J. Phys. 20, 100 (1946).
[15] M. M. Patel, S. P. Patel, and A. B. Darji, Ind. J. Pure Appl. Phys. 5, 566 (1967).
[16] R. K. Gosavi, G. Greig, P. J. Young, and O. P. Strausz, J. Chem. Phys. 34, 983 (1970).
[17] B. Rosen, *Spectroscopic Data Relative to Diatomic Molecules* (Pergamon, Oxford, 1970), p. 118.
[18] J. Tellinghuisen, A. K. Hays, J. M. Hoffman, and G. C. Tisone, J. Chem. Phys. 65, 4473 (1976); J. Tellinghuisen and R. J. Exton, J. Phys. B 13, 4781 (1980); J. Tellinghuisen, P. Berwanger, J. G. Ashmore, and K. S. Viswanathan, Chem. Phys. Lett. 84, 528 (1981).
[19] A. Mandl and J. H. Parks, Rev. Sci. Instrum. 50, 127 (1979).
[20] J. Tellinghuisen and J. G. Ashmore, Appl. Phys. Lett. 40, 867 (1982).

To be published in
J. Opt. Soc. Am. B

EXCITATION OF THE HgBr $B^2\Sigma^+_{1/2} \rightarrow X^2\Sigma^+_{1/2}$ BAND IN THE ULTRAVIOLET

D. P. Greene*, K. P. Killeen† and J. G. Eden

University of Illinois
Urbana, IL 61801

ABSTRACT

The buildup and decay of the HgBr $X^2\Sigma^+_{1/2}$ species during a pulsed discharge in Ne, N_2 and $HgBr_2$ vapor and in its afterglow have been examined by monitoring $B^2\Sigma^+_{1/2} \rightarrow X^2\Sigma^+_{1/2}$ absorption by the discharge at 351 nm. Also, the UV-to-green conversion efficiency for the 350 nm-pumped HgBr laser is shown to be sensitive to the 502 nm fluence circulating in the cavity when the XeF laser pump pulse arrives. The maximum observed efficiency (η) of 22% is obtained for intracavity intensities of 1 to 2 MW - cm^{-2} but η falls to ~ 10% for I ≈ 1 kW - cm^{-2}.

*Present address: Laser Physics Group (P16), MS 523, Los Alamos National Laboratory, P. O. Box 1663, Los Alamos, NM 87545.
†Present address: Org. 1126, Sandia National Laboratory, P. O. Box 5800, Albuquerque, NM 87185
PACS Nos.: 42.55.Hq, 33.20.Lg

I. INTRODUCTION

In an earlier paper[1], experiments were reported in which absorption by diatomic HgBr radicals on the near-ultraviolet (UV), B ← X band was exploited to efficiently convert XeF (351 nm) or frequency-tripled Nd: YAG (355 nm) laser radiation into the green (502 nm). Carried out in the active medium of a discharge-pumped HgBr laser, these experiments reproducibly demonstrated UV-to-green energy conversion efficiencies (η) exceeding 20%. This paper presents more detail regarding the temporal behavior of the HgBr ground state population and the structure of the B ← X absorption band.

Figure 1 shows the spectral profile for the $B^2\Sigma^+_{1/2} \leftarrow X^2\Sigma^+_{1/2}$ absorption band of HgBr that was recorded in the afterglow of a pulsed, transverse discharge containing Ne, N_2 and $HgBr_2$ (natural abundance) vapor. This spectrum was obtained with an optical multichannel analyzer (OMA) and a pulsed xenon flashlamp having a pulsewidth of ~ 300 ns FWHM. Details of the technique used in making these measurements can be found in ref. 2. Peaking in the ultraviolet between 340 and 360 nm, the band falls off slowly towards the red and has a spectral width of ~ 60 nm FWHM. While the majority of the profile is essentially a continuum, the structure near the band peak is real.

II. HgBr (B ← X) ABSORPTION BAND: VIBRATIONAL STRUCTURE

Table I lists the wavelengths, energies ($\tilde{\nu}$, in cm^{-1}) and tentative vibrational assignments for the 18 strongest features in the spectrum of Fig. 1. (A detailed view of this region is given in Fig. 2). The average separation between adjacent bandheads is 113 ± 8 cm^{-1} (uncertainty represents one standard deviation). Using this value and the vibrational constants for the B state that were reported by Tellinghuisen and Ashmore[3] yields an estimate of $v' \approx 45$ for

the vibrational quantum number of the upper state that corresponds to the most intense peak in the B → X absorption band (Figs. 1, 2).

Table I also lists the energies calculated with the vibrational constants of ref. 3 for transitions from v" = 0 of the ground state to the $32 \leq v' \leq 50$ vibrational levels of the B state. If one tentatively assigns these transitions to the bandheads observed in Figs. 1 and 2, then only the v' = 39 → v" = 0 transition appears to be missing from the progression. However, the average value of $\Delta\tilde{\nu}(\equiv\tilde{\nu}_{calc} - \tilde{\nu}_i)$ for the first eleven transitions in Table I is unacceptably large ($\overline{\Delta\tilde{\nu}_i} = 39 \pm 5$ cm^{-1}) which may be due to an incorrect assignment. Another possibility is to attribute the entire discrepancy to not having accounted for $\omega_e y_e$ (coefficient for the cubic term in the series expansion for the B state vibrational level energies) in the computation of $\tilde{\nu}_{calc}$. If this is the case, the data for the v' = 50 → v" = 0 to 40 → 0 vibrational transitions suggest that $\omega_e y_e$ lies in the range $3 \cdot 10^{-4} \lesssim \omega_e y_e \leq 6 \cdot 10^{-4}$ cm^{-1}. Clearly, higher resolution spectroscopic experiments will be necessary to resolve this issue.

III. EXPERIMENTAL APPARATUS

A schematic diagram of the experimental apparatus used to examine the buildup and decay of the HgBr ground state ($X^2\Sigma^+_{1/2}$) number density in an HgBr laser discharge is given in Figure 3. A 16 ns FWHM, 351 nm pulse from a "free-running" XeF laser was directed along the axis of the transverse discharge and the energy in the pulse was measured before entering and after leaving the cell. Untuned, the laser oscillates on two molecular transitions which lie at 351.1 and 353.1 nm. The majority of the total pulse energy is contained in a narrow peak at 351.14 nm whose spectral width is ~ 5 cm^{-1}.

Design and construction details for the 50 cm active length discharge device can be found elsewhere[4,5]. It must be emphasized that the major role of the discharge in these experiments is to provide a pulsed source of $HgBr(X^2\Sigma)$ radicals. For all of the experiments discussed here, the gas mixture included: $[Ne] = 3.8 \cdot 10^{19}$ cm^{-3}, $[N_2] = 3.2 \cdot 10^{18}$ cm^{-3} and $[HgBr_2] = 4.1 \cdot 10^{16}$ cm^{-3} (T = 420°K). Also, the storage capacitance was 20 nF and, for a charging voltage of 30 kV, the peak current was ~ 10 kA and the maximum instantaneous power loading of the medium was 1 to 2 MW - cm^{-3}. A simple telescope composed of two cylindrical lenses compressed the rectangular (1.0 × 2.5 cm^2) excimer laser beam down to a cross-sectional area of 0.4 cm^2 (1.0 × 0.4 cm^2) so as to match the area of the active medium produced by the discharge. The beam was also spatially filtered before entering the discharge cell. Varying the timing between the firing of the XeF laser and the discharge was accomplished with digital delay generators. In the initial experiments described here (Figures 4 - 10), the optical cavity shown in Figure 3 was <u>not</u> in place. However, with an optical cavity having a low Q at 502 nm installed around the discharge (R_1 = 99% at 502 nm, R_2 = 16% at 502 nm; 3m radii of curvature, separated by 1m), the laser normally produced 17 mJ, ~40 ns FWHM pulses. As mentioned earlier, when acquiring the transient absorption spectra described in the next section, a pulsed Xe lamp was placed in front of the laser discharge and an OMA acted as the detector.

IV. RESULTS

A. Transient Absorption Spectra

The transient absorption spectrum of the HgBr laser plasma in the visible and UV($240 \leq \lambda \leq 520$ nm) at different times in the afterglow is illustrated in

Fig. 4. The time delay Δt between maximum discharge current and the peak in the Xe lamp pulse is indicated for each spectrum. Also, the spectral profiles are the result of time-integrating over the width of the Xe lamp probe pulse (300 ns). Consequently, even the $\Delta t = 0$ spectrum samples ~70 ns into the afterglow (discharge current FWHM ~60 ns, power pulse terminates ~80 ns after peak current).

The region above the dashed line in each of the three segments of Fig. 4 represents absorption whereas excursions below the horizontal line reflect optical gain. However, the latter does not hold for $\lambda \lesssim 300$ nm. That is, the apparent "gain" between the C → X and D → X bands of HgBr (centered at 285 and 255 nm, respectively) actually arises from the increased transparency of the discharge medium in this spectral region due to transient depletion of the $HgBr_2$ concentration by electron impact dissociation. The procedure for acquiring spectra such as those in Fig. 4 involves normalizing the raw data to the transmission spectrum recorded before the discharge is fired. However, as indicated in Fig. 5, $HgBr_2$ vapor absorbs strongly for wavelengths below ~300 nm because of the $1^1\Pi_u \leftarrow 1^1\Sigma_g$ continuum[6-8]. Therefore, the reduction in the instantaneous $HgBr_2$ density during the discharge and its afterglow yields apparent gain in the UV. Finally, the C and D states of HgBr are also clearly observed in emission as shown in Fig. 6.

B. HgBr(X) Kinetics

The temporal history of the strength of the X → B band of HgBr, monitored at 351 nm, is illustrated in Figure 7. In taking these data, the 351 nm energy absorbed by the discharge was recorded as a function of time delay (Δt) between the firing of the discharge and the entry of a UV laser pulse into the plasma. An XeF laser, rather than an incoherent source, was chosen as the optical probe

because of the difficulties associated with propagating an incoherent beam through the small cross-sectional area, 50 cm long plasma. Also, the XeF laser intensity was maintained at ~0.6 MW-cm^{-2} in order to avoid saturation effects (cf. Fig. 8).

Probing the X → B absorption band in the vicinity of 351 nm ensures that one is observing the lowest-lying vibrational levels (i.e., v" = 0, 1) of the ground state[9,10] while, at the same time, producing v' ≈ 40-50 levels in the ionic $B^2\Sigma^+_{1/2}$ state[11]. Therefore, we associate the data of Figure 7 with the buildup and decay of the population of the $X^2\Sigma$ (v" = 0,1) vibrational levels during and immediately following the discharge. At this point, it should be mentioned that since the relaxation of the HgBr ground state vibrational manifold is known to be rapid[10], then early in the afterglow of the discharge, the bulk of the X state vibrational population is expected to reside in the lowest states. This conclusion is consistent with the observation that no noticeable change occurs in the B → X spectrum for $\Delta t \gtrsim 100$ ns (cf. Fig. 4).

Clearly, the HgBr ground state concentration rises rapidly during the life of the discharge and peaks shortly thereafter. Beyond $\Delta t \sim 0.3$ μs, however, [HgBr(X)] falls rapidly, owing primarily to reformation of the $HgBr_2$ "parent" molecule. The decay of the X state number density in this region is well-described by a single exponential having a time constant of $\tau \approx 0.8$ μs.

Erlandson and Cool[9] have attributed the regeneration of $HgBr_2$ in HgBr photodissociation lasers to the bimolecular reaction:

$$HgBr + Br_2 \xrightarrow{k_1} HgBr_2 + Br \qquad (1)$$

and measured k_1 to be $(7.7 \pm 0.6)\cdot 10^{-11}$ cm^3 - s^{-1} at 415°K. However, for reaction (1) to account for the decay of the data in Figure 7 would require a

Br_2 concentration in the discharge of $\sim 2 \cdot 10^{16}$ cm^{-3} or approximately 0.7 Torr at 415°K. Attaining such a large Br_2 number density only a few hundred nanoseconds into the afterglow is not only unlikely but no evidence of Br_2 transient absorption (in spectra such as Fig.4) has yet been observed.

Alternative explanations for the 0.8 μs decay include the loss of HgBr radicals by:

a) Three body collisions:

$$HgBr(X^2\Sigma) + Br + Ne \xrightarrow{k_2} HgBr_2 + Ne \quad , \tag{2}$$

b) Two body collisions involving pairs of HgBr(X) radicals:

$$HgBr(X^2\Sigma) + HgBr(X^2\Sigma) \rightarrow HgBr_2 + Hg \tag{3}$$

c) Electron impact dissociation,

or

d) Dissociative attachment:

$$HgBr(X) + e^- \rightarrow Hg + Br^- \quad . \tag{4}$$

The rapid thermalization of electrons in the discharge afterglow suggests that c) can be ignored. For an estimated Br density of 10^{14} cm^{-3} and [Ne] = $3.8 \cdot 10^{19}$ cm^{-3}, then k_2 would be $3(\pm 1) \cdot 10^{-28}$ $cm^6 - S^{-1}$ if reaction (2) were totally responsible for the [HgBr(X)] decay shown in Fig. 7. It is more likely that both (1) and (4) are responsible for the removal of ground state diatomic radicals since (4) only requires the presence of cool electrons. Reaction (3) becomes a significant loss mechanism only if its rate constant is gas kinetic.

The dependence of the HgBr ground state absorption (at 351 nm) on the XeF laser intensity is shown in Fig. 8. Note that Δt = 108 ns (i.e., corresponding to the peak of Fig. 7) and that the data varies linearly with I_{XeF} over the intensity range investigated (as indicated by the linear least squares fit to the data (solid line). The absence of any indication of saturation in Fig. 8 is reasonable since, even at the highest XeF pulse energies studied (35 mJ), the 351 nm fluence is insufficient to significantly deplete the HgBr ($X^2\Sigma$) population (estimated to exceed 10^{16} in the ~10 cm^3 active volume of the discharge). It is expected, however, that for higher XeF laser intensities, ground state depletion would become noticeable and the slope of the data (presently 0.2 for the points given in Fig. 8) would tend toward unity.

C. Flashlamp and Laser Pumping of HgBr (B → X) Band

As illustrated in Figure 9, the gain spectrum of the HgBr (B → X) band was also monitored, again using the pulsed Xe lamp and the OMA system. By varying the time at which the lamp fired with respect to the HgBr discharge, the temporal evolution of the gain spectrum could be observed. A UV-cutoff, glass filter which passed only radiation of $\lambda \geq 395$ nm was placed between the pulsed lamp and the discharge. As expected, strong gain is observed at Δt = 0 (peak discharge current) since HgBr(B) molecules are being produced in the discharge by electron impact, dissociative excitation of $HgBr_2$. Also, the structure in the gain spectrum replicates that of the B → X spontaneous emission profile (Fig. 6) near its peak. However, owing to the ~25 ns radiative lifetime of the HgBr(B) state and the 50-60 ns width of the discharge's power (V·I) pulse, all evidence of gain has vanished at Δt = 450 ns.

If one, however, removes the UV absorbing filter, then (as shown in Figure 10) significant gain is observed at times late in the discharge afterglow

($\Delta t > 1$ μs). The logical interpretation of this result is that UV radiation from the pulsed lamp is pumping the X → B transition of HgBr, leading to the subsequent appearance of gain at 502 nm. As can be seen from Figure 7, the HgBr ground state concentration at $\Delta t = 450$ ns is a large fraction (~ 75%) of its peak value.

In subsequent experiments, the optical cavity shown in Figure 3 was installed around the discharge cell. Both mirrors had a 3 m radius of curvature and the XeF pulse was injected into the cavity via a mirror which transmitted 90% at 351 nm. In the absence of the external UV laser pulse, intense lasing on the B → X band of HgBr occurred upon firing the discharge. In this case, of course, the inversion between v' = 0, 1 of the $B^2\Sigma^+_{1/2}$ state and high-lying vibrational levels (v" = 22, 23) of ground is produced solely by electron impact, dissociative excitation of the HgBr(B) state from the $HgBr_2$ parent molecule. The dynamics of this mechanism, as well as the dissociative $HgBr_2^*$ states involved, have been previously studied by several groups[12-14]. The FWHM of this first laser pulse is 40 - 45 ns. The arrival of the XeF radiation produces a second blue-green laser pulse having the same temporal width as that for the 351 nm laser waveform[1].

As was reported in ref. 1, the conversion of 351 nm energy into 502 nm photons is efficient (22 ± 1% for $\Delta t = 90 \pm 8$ ns). Figure 11 shows the linear relationship between XeF energy absorbed by the discharge and the additional 502 nm energy that emerges from the optical cavity. By "additional" we mean the radiation above and beyond that produced by the discharge alone.

The UV-to-green energy conversion efficiency (η) is a strong function of Δt as illustrated in Figure 12 (for $E_{XeF} = 26$ mJ). For $\Delta t \lesssim 60$ ns, η closely follows the rapid rise in the HgBr ground state population. However, the energy

conversion efficiency falls much more rapidly beyond Δt = 90 ns than one would expect from Figure 7 (HgBr(X) concentration, [HgBr(X)]). At Δt = 180 ns, lasing in the green has nearly vanished although [HgBr(X)] is still 92% of its peak value. The discrepancy between the HgBr(X) population and the rapid drop in η is illustrated in Figure 7 where the dashed line indicates the decline in η for $\Delta t > 90$ ns. The problem is that, for $\Delta t > 90$ ns, the first HgBr laser pulse (produced by the discharge) has been emitted (first pulse ceases at $\Delta t \sim 80$–90 ns) and the residual 502 nm intracavity fluence I has dwindled to the point where $I \ll I_{sat} \sim 200$ kW - cm^{-2} (ref. 15). Therefore, as Δt rises, an increasing percentage of the 351 nm pump fluence must be expended to reach threshold by overcoming spontaneous and non-radiative (quenching) losses from the B state. For the mirrors used in these experiments, the optical cavity lifetime (at 502 nm) is ~8 ns (cavity length = 1 m) and a second laser pulse is observed up to ~ 10 cavity lifetimes beyond the termination of the first laser pulse. The peak instantaneous intracavity intensity during the discharge-produced laser pulse (i.e., first pulse) is typically 2 MW - cm^{-2}. Consequently, it appears that the 502 nm fluence circulating in the cavity when the XeF pump pulse arrives must exceed ~ 1.0 kW - cm^{-2} in order to obtain conversion efficiencies above ~ 10%.

In conclusion, the buildup and decay of the $X^2\Sigma^+_{1/2}$ number density during and after a pulsed $Ne/N_2/HgBr_2$ has been examined by monitoring absorption by the plasma at 351 nm. Also, temporal studies of the 351 nm - pumped HgBr laser at 502 nm confirm that realizing the maximum UV-to-green conversion efficiency (22% requires that the intracavity 502 nm fluence be sufficiently large to overcome spontaneous emission and quenching losses from the B state.

The authors appreciate the excellent technical assistance of K. Kuehl, A. B. Wilson, Y. Moroz and D. Watterson. Special thanks are extended to C. C. Abele for his assistance in the acquisition and analysis of the data by computer. This work was supported by the National Science Foundation (J. Aller, L. Goldberg) under grant ECS 83-09641 and the Army Research Office (B. Guenther) under contract DAAG 29-83-K-0108.

REFERENCES

1. D. P. Greene, K. P. Killeen and J. G. Eden, "$X^2\Sigma \rightarrow B^2\Sigma$ absorption band of HgBr: Optically-pumped 502 nm laser," Appl. Phys. Lett. 48, 1175 (1986).
2. D. P. Greene and J. G. Eden, "Transient absorption in a cadmium monoiodide laser discharge," Opt. Comm. 53, 263-268 (1985).
3. J. Tellinghuisen and J. G. Ashmore, "Mixed representations for diatomic spectroscopic data: Application to HgBr," Chem. Phys. Lett. 102, 10-16 (1983).
4. D. P. Greene and J. G. Eden, "Discharge pumped ZnI (599 - 606 nm) and CdI (653-662 nm) amplifiers," Appl. Phys. Lett. 42, 20-22 (1983).
5. D. P. Greene and J. G. Eden, "Lasing on the B → X band of cadmium monoiodide (CdI) and ^{114}CdI in a UV-preionized, transverse discharge," Appl. Phys. Lett. 43, 418-420 (1983).
6. W. R. Wadt, "The electronic structure of $HgC\ell_2$ and $HgBr_2$ and its relationship to photodissociation," J. Chem. Phys. 72, 2469-2478 (1980).
7. C. Roxlo and A. Mandl, "Vacuum ultraviolet absorption cross sections for halogen containing molecules," J. Appl. Phys. 51, 2969 (1980).
8. D. Spence, R. G. Wang and M. A. Dillon, "Pseudo-optical absorption spectra in $HgC\ell_2$ and $HgBr_2$ from 4 to 14 eV," Appl. Phys. Lett. 41, 1021-1023 (1982).
9. A. C. Erlandson and T. A. Cool, "On the regeneration mechanism of $HgBr_2$ in $HgBr/HgBr_2$ dissociation lasers," Chem. Phys. Lett. 96, 685-689 (1983).
10. H. Helvajian and C. Wittig, "Vibration quenching of $HgBr(X^2\Sigma^+_{1/2})$," Appl. Phys. Lett. 38, 731-733 (1981).
11. N. H. Cheung and T. A. Cool, "Franck-Condon factors and r-centroids for the $B^2\Sigma - X^2\Sigma$ systems of HgCℓ, HgBr and HgI," J. Quant. Spectrosc. Radiat. Transfer 21, 397-432 (1979).

12. E. J. Schimitschek and J. E. Celto, "Mercuric bromide dissociation laser in an electric discharge," Opt. Lett. 2, 64-66 (1978).

13. R. Burnham, "Discharge pumped mercuric halide dissociation lasers," Appl. Phys. Lett. 33, 156-159 (1978).

14. W. L. Nighan, "Kinetic processes in the electrically excited mercuric bromide dissociation laser," Appl. Phys. Lett. 36, 173-175 (1980).

15. E. J. Schimitschek and J. E. Celto, "Oscillator and oscillator-amplifier experiments with an $HgBr_2$/HgBr dissociation laser," Appl. Phys. Lett. 36, 176-178 (1980).

TABLE I.

OBSERVED BANDHEADS IN THE $B^2\Sigma^+_{1/2}(v') \rightarrow X^2\Sigma^+_{1/2}(v'')$ ABSORPTION SPECTRUM OF HgBr. THE WAVELENGTHS GIVEN IN THE SECOND COLUMN FROM THE LEFT WERE MEASURED IN AIR.

Bandhead No. (i)	λ (nm)	$\tilde{\nu}_i$ (cm^{-1})	$\tilde{\nu}_i - \tilde{\nu}_{i+1}$	$\tilde{v}', v''$	$\tilde{\nu}_{calc}$ (cm^{-1})	$\Delta\tilde{\nu}_i = \tilde{\nu}_{calc} - \tilde{\nu}_i$
1	338.05	29573.0	113.3	50,0	29611.6	38.6
2	339.35	29459.7	100.4	49,0	29501.1	41.4
3	340.51	29359.3	123.6	48,0	29390.1	30.8
4	341.95	29235.7	110.7	47,0	29278.6	42.9
5	343.25	29125.0	109.9	46,0	29166.5	41.5
6	344.55	29015.1	120.8	45,0	29054.0	38.9
7	345.99	28894.3	107.3	44,0	28940.9	46.6
8	347.28	28787.0	107.4	43,0	28827.4	40.4
9	348.58	28679.6	124.5	42,0	28713.3	33.7
10	350.10	28555.1	107.2	41,0	28598.7	43.6
11	351.42	28447.9	-----	40,0	29483.6	35.7
--	------	-------	-----	39,0	28368.0	
12	354.05	28236.6	104.1	38,0	28251.9	
13	355.36	28132.5	115.1	37,0	28135.3	
14	356.82	28017.4	125.9	36,0	28018.1	
15	358.43	27891.5	112.4	35,0	27900.5	
16	359.88	27779.1	112.2	34,0	27782.4	
17	361.34	27666.9	110.6	33,0	27663.7	
18	362.79	27556.3	-----	32,0	27544.5	

$$\overline{\tilde{\nu}_i - \tilde{\nu}_{i+1}} = 112.8 \pm 7.5 \text{ cm}^{-1}$$

FIGURE CAPTIONS

Figure 1. Time-integrated spectral profile of the HgBr $B^2\Sigma^+_{1/2} \rightarrow X^2\Sigma^+_{1/2}$ absorption band recorded ~1.1 μs into the afterglow of the discharge. The spectral resolution of the detection system is ~ 0.1 nm and the structure near the band peak ($330 \leq \lambda \leq 370$ nm) is real. The Ne, N_2 and $HgBr_2$ number densities are $3.8 \cdot 10^{19}$ cm^{-3}, $3.2 \cdot 10^{18}$ cm^{-3} and $4.1 \cdot 10^{16}$ cm^{-3}, respectively.

Figure 2. Expanded view of the bandheads near the peak of the HgBr (B → X) absorption spectrum (Fig. 1). For convenience, the individual peaks are numbered according to the order in which they appear in Table I.

Figure 3. Diagram of the experimental apparatus. The relative timing between the firing of the excimer laser and the HgBr discharge could be adjusted with digital delay generators (not shown).

Figure 4. Transient absorption spectrum of the $Ne/N_2/HgBr_2$ discharge for $240 \leq \lambda \leq 520$ nm and at different times following peak discharge current.

Figure 5. $HgBr_2$ $1^1\Pi_u \rightarrow 1^1\Sigma_g$ absorption spectrum in the ultraviolet ($240 \leq \lambda \leq 320$ nm). These data were acquired with the same apparatus used in obtaining Figs. 1, 2 and 4 and the spectral resolution is ~0.1 nm.

Figure 6. Spontaneous emission spectrum of the $Ne/N_2/HgBr_2$ discharge for $240 \leq \lambda \leq 540$ nm. The resolution is again ~0.1 nm and key spectral features are identified.

Figure 7. Temporal variation of the HgBr ground state absorption at 351 nm ($X^2\Sigma^+_{1/2}$, v' = 0,1) for [Ne] = $3.8 \cdot 10^{19}$ cm^{-3}, [N_2] = $3.2 \cdot 10^{18}$ cm^{-3} and [$HgBr_2$] = $4.1 \cdot 10^{16}$ cm^{-3}. The XeF laser pulse energy was held constant at 26 ± 2 mJ. Note that absorption is nearly constant for $80 \leq \Delta t \leq 200$ ns and, as shown by the solid curve, decays exponentially with a time constant of ~ 0.8 μs. The dashed line will be discussed later in the text (in conjunction with Fig. 12).

Figure 8. Energy of the transmitted 351 nm pulse as a function of the beam energy incident on the Ne/N_2/$HgBr_2$ discharge. The line (slope = 0.2) represents the linear least squares fit to the data. The Ne, N_2 and $HgBr_2$ densities are the same as those for Fig. 7.

Figure 9. Small signal gain spectrum for the B → X band of HgBr: (a) during the active discharge and (b) 450 ns into the afterglow. In acquiring these spectra, UV radiation from the Xe probe lamp was blocked from reaching the discharge by a glass filter.

Figure 10. Same spectra as Fig. 9 but with the UV-absorbing filter removed from the optical path. The gain now evident in the green for Δt = 450 ns is due to the pulse lamp pumping the 350 nm-centered B → X band of HgBr.

Figure 11. Conversion of absorbed XeF (351 nm) radiation into the green (λ = 502 nm). For these data, Δt was fixed at 90 ± 8 ns.

Figure 12. Temporal history of the UV-to-green energy conversion efficiency for E_{XeF} fixed at 26 ± 2 mJ. Note the rapid decline in efficiency beyond Δt ≈ 90 ns. The termination of the first HgBr laser pulse (not shown) occurs at Δt = 80-90 ns.

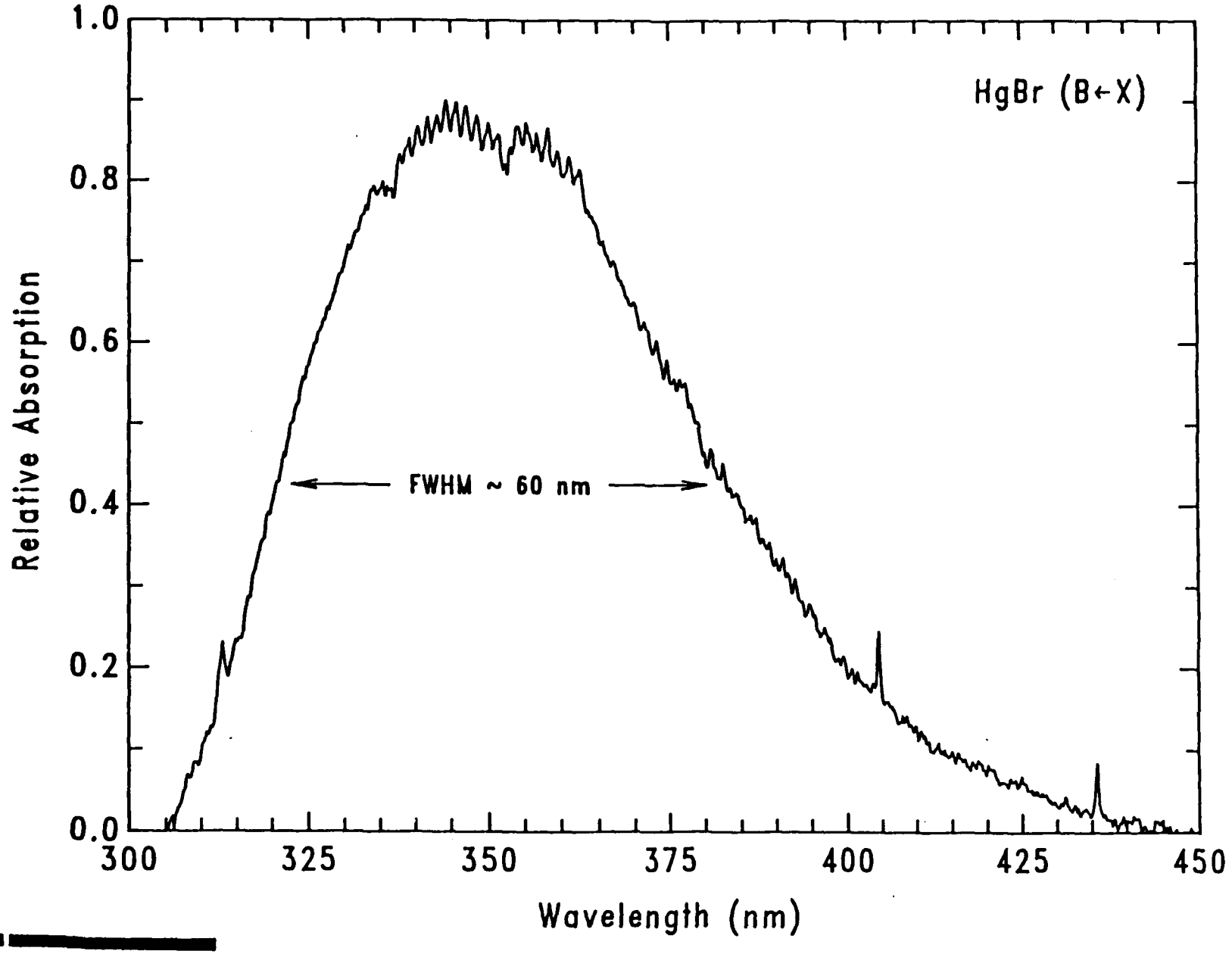

Fig. 1
Greene et. al.

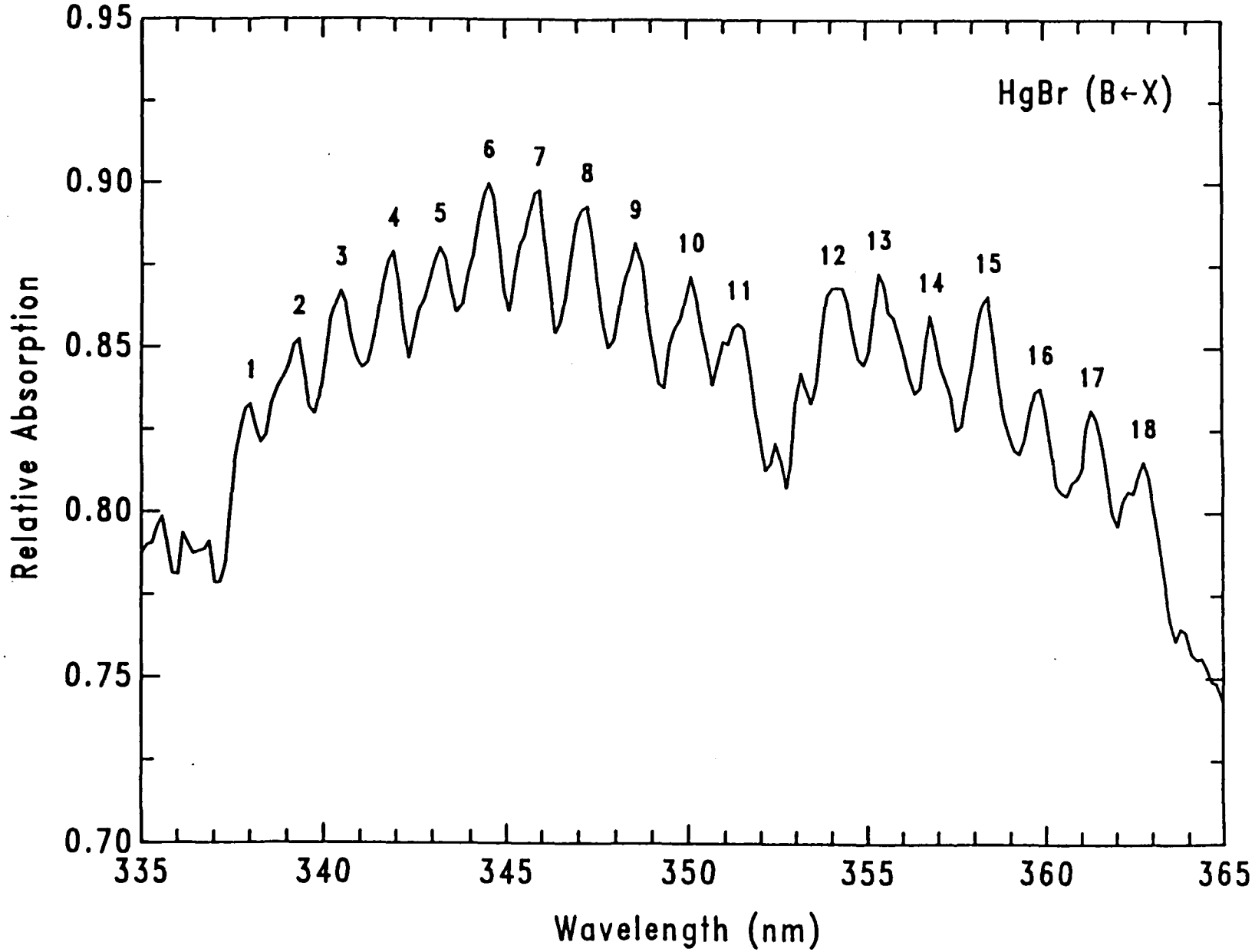

Fig. 2
Greene et. al.

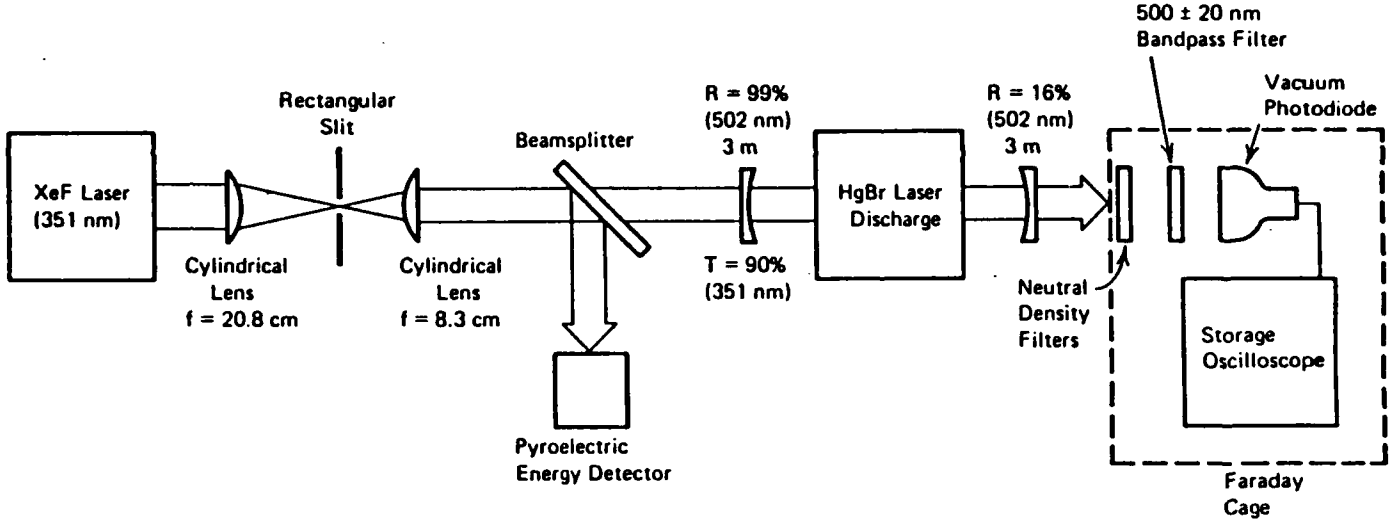

Fig. 3

Greene et. al.

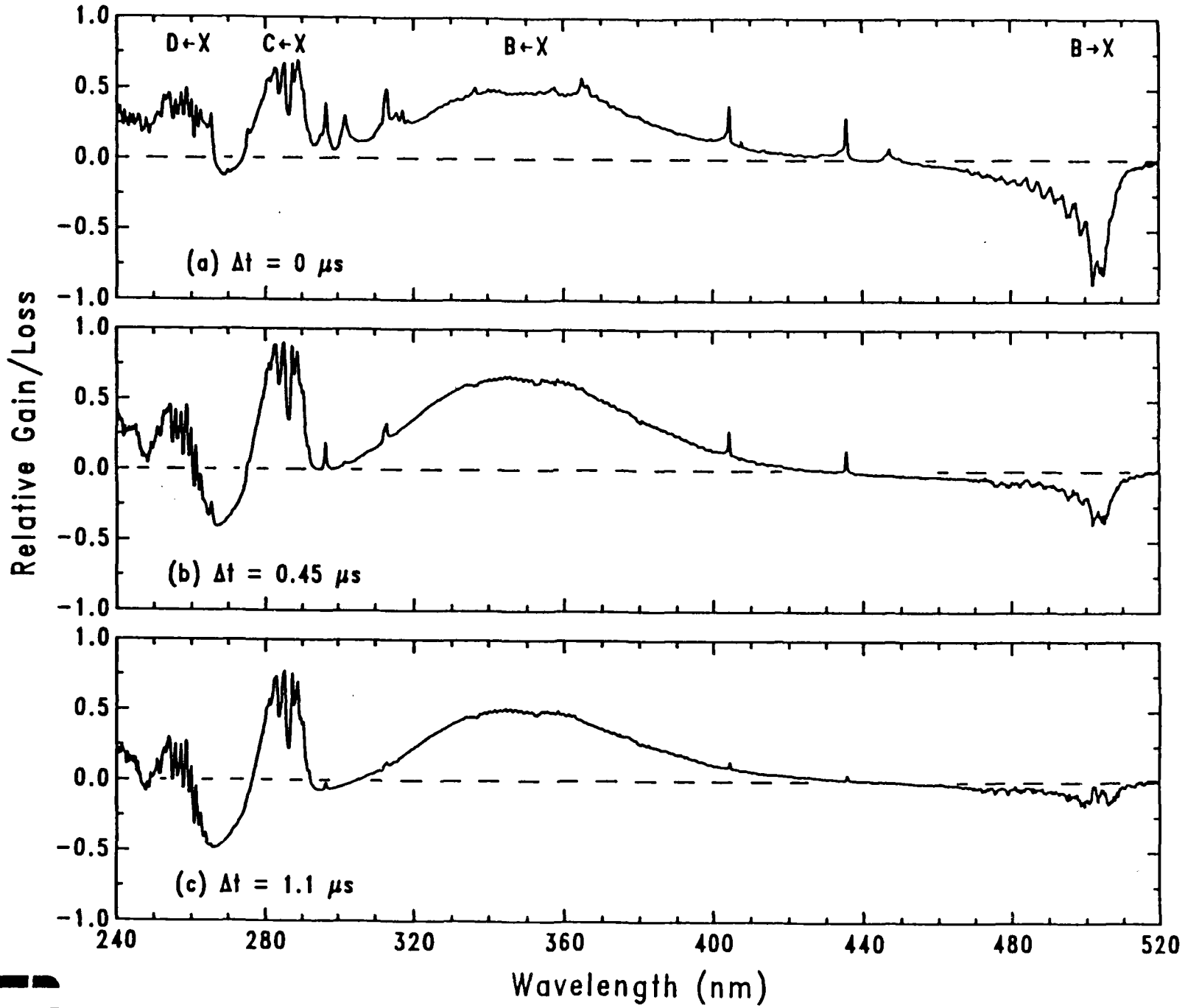

Fig. 4

Greene et. al.

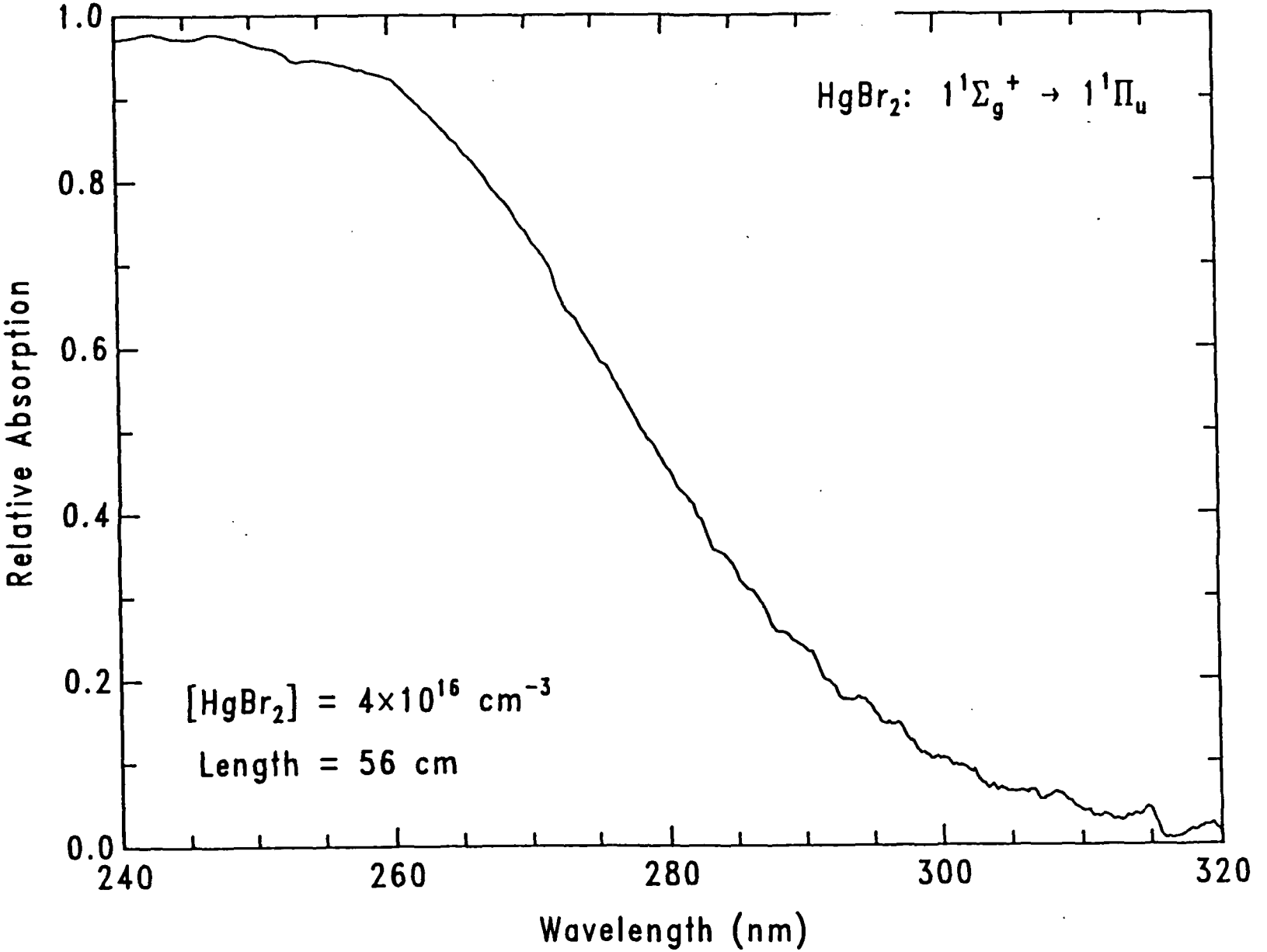

Fig. 5
Greene et. al.

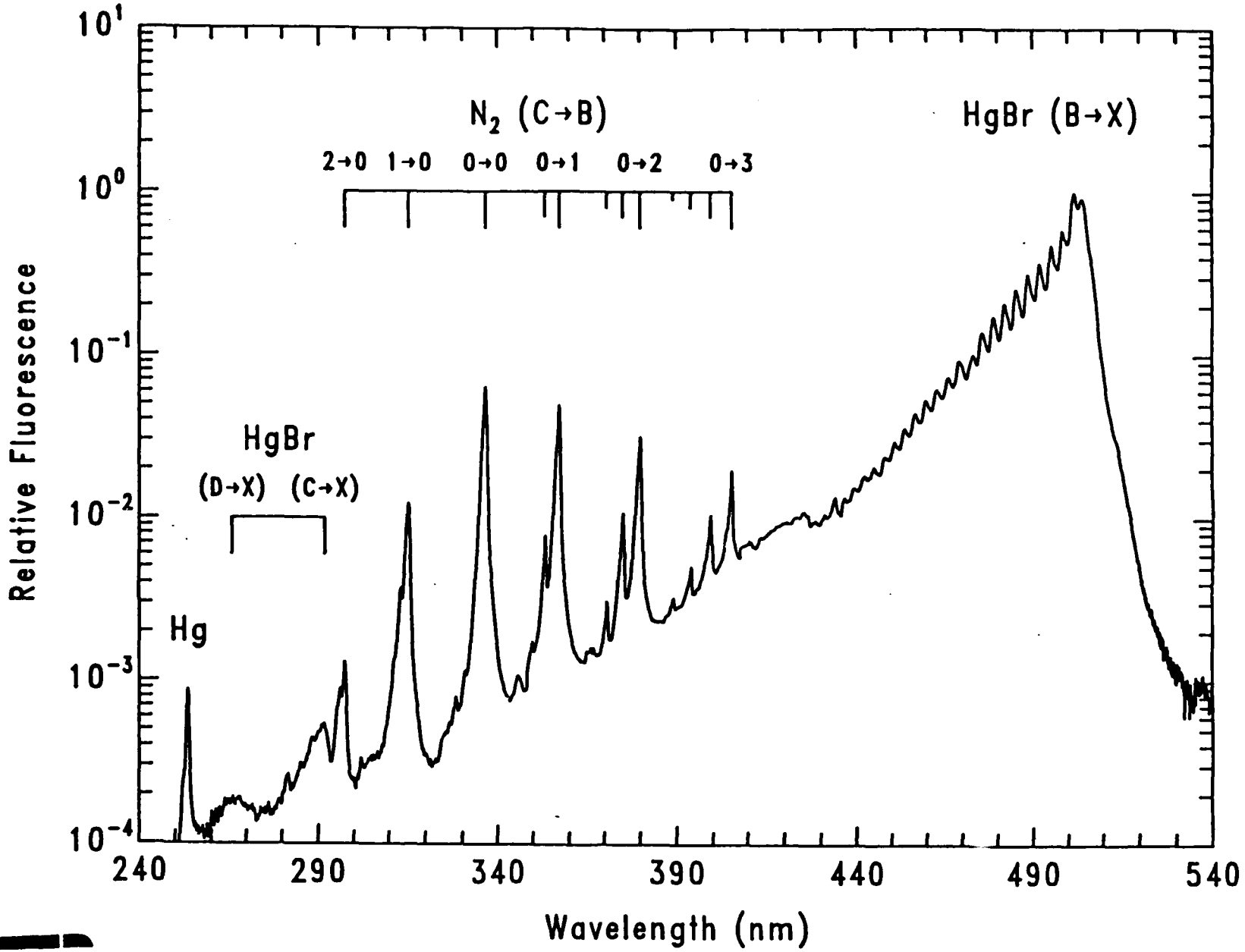

Fig. 6
Greene et. al.

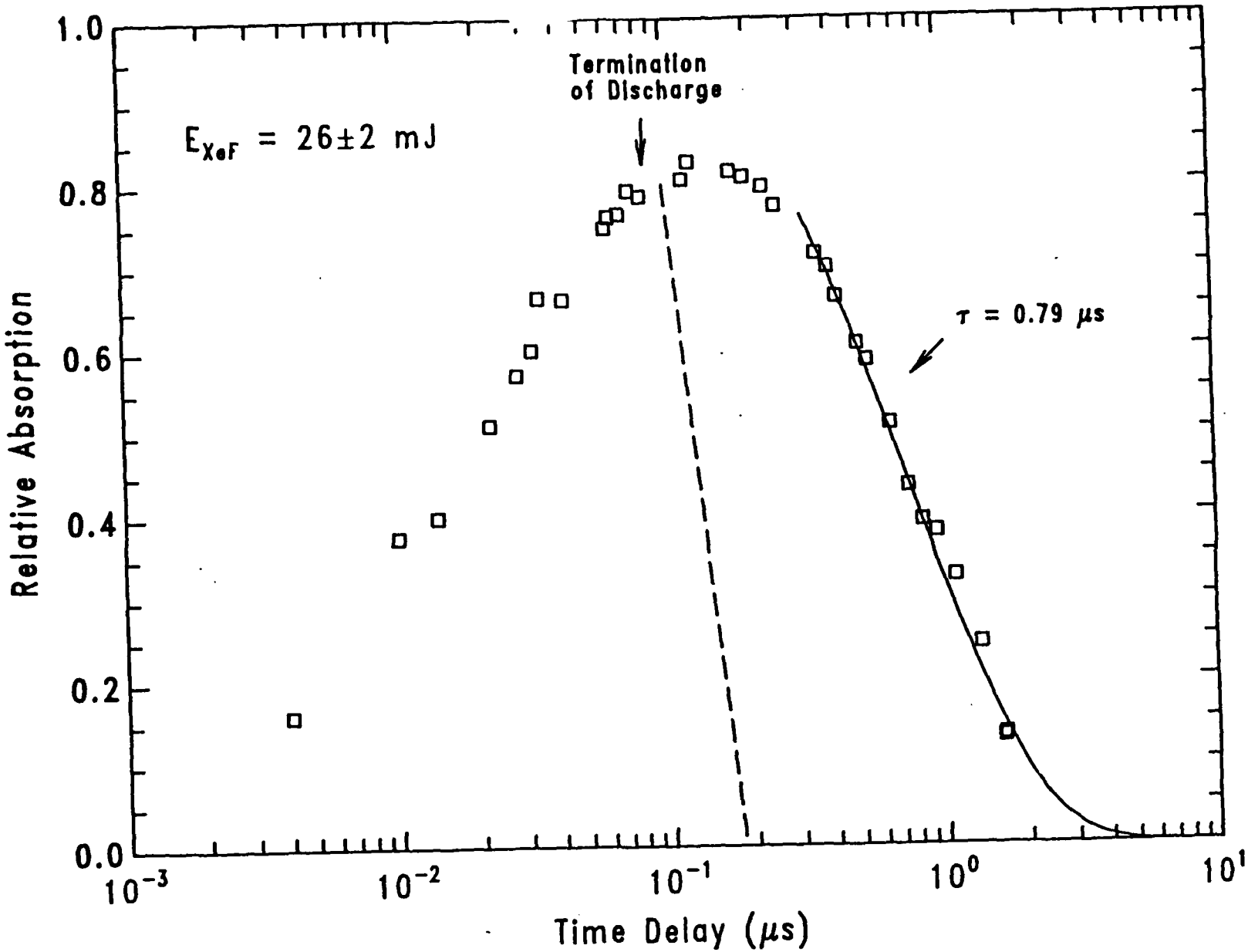

Fig. 7
Greene et. al.

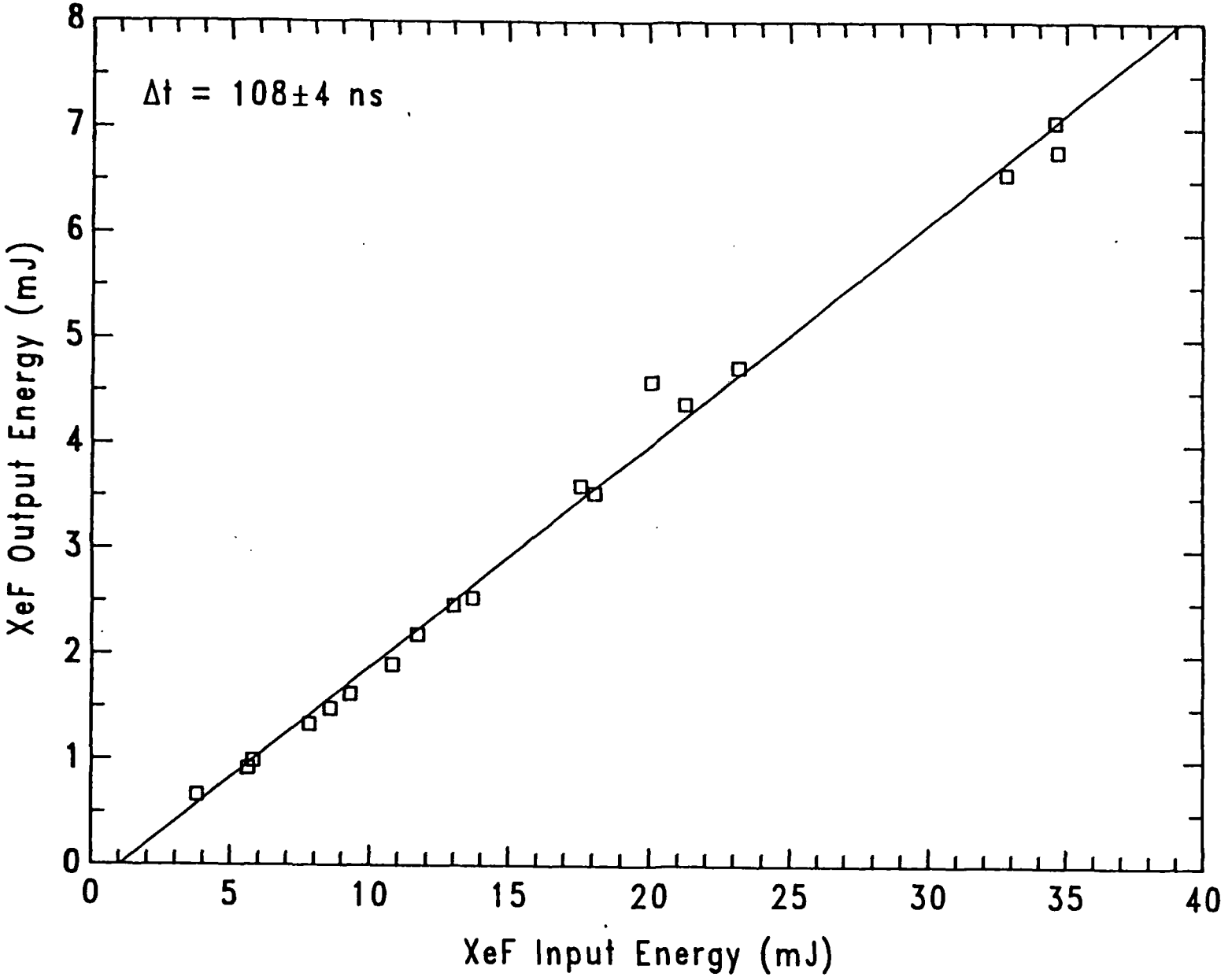

Fig. 8
Greene et. al.

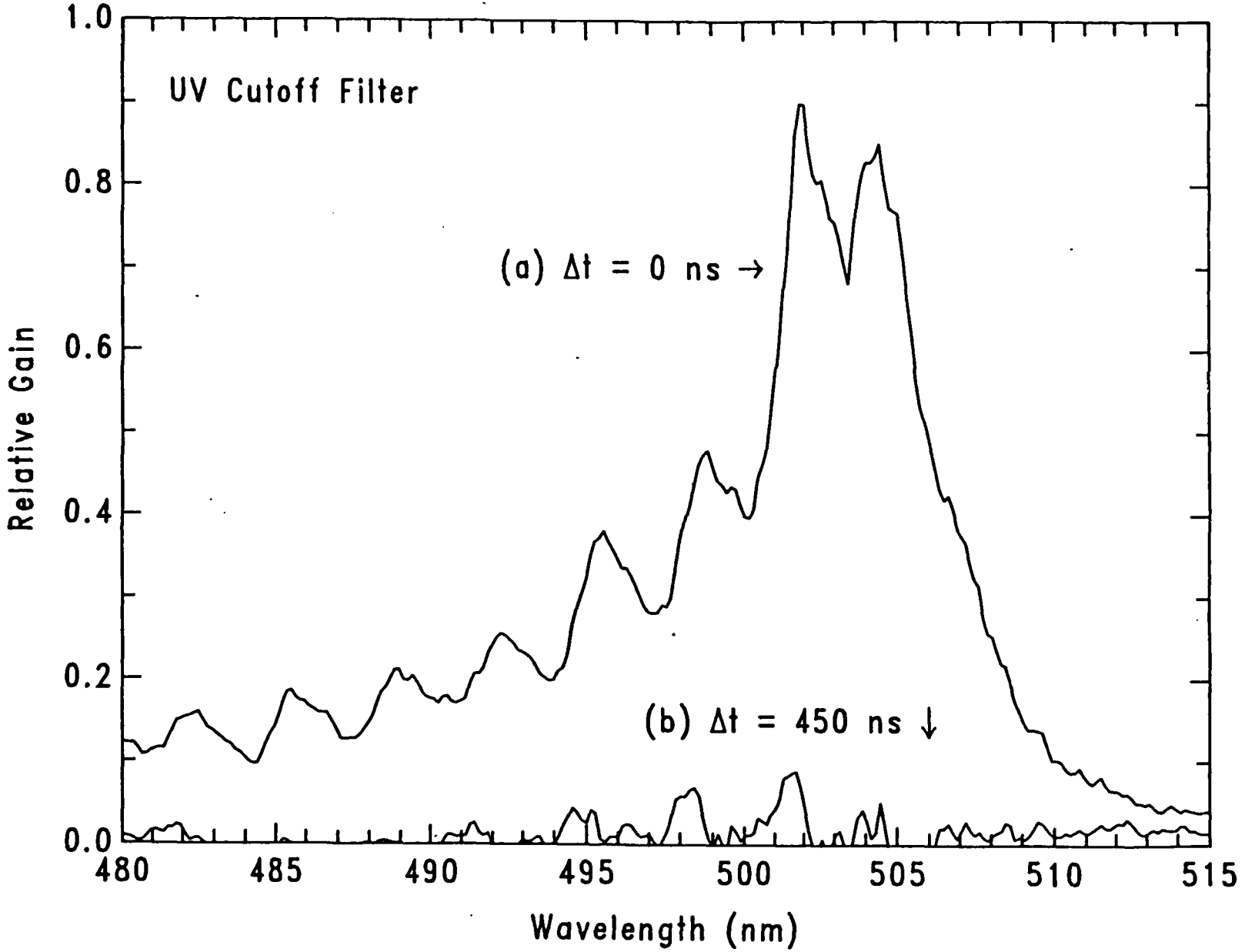

Fig. 9
Greene et. al.

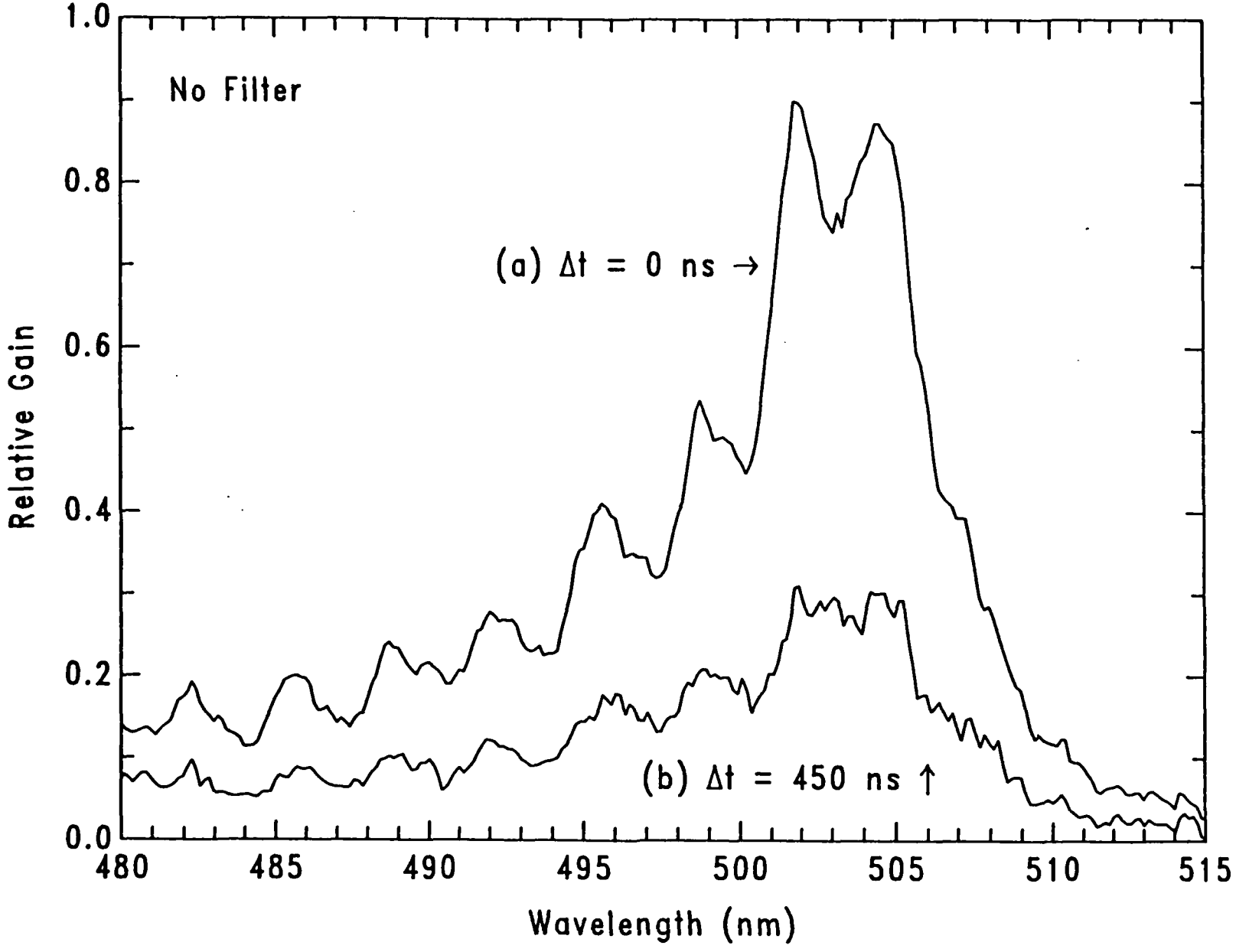

Fig. 10
Greene et. al.

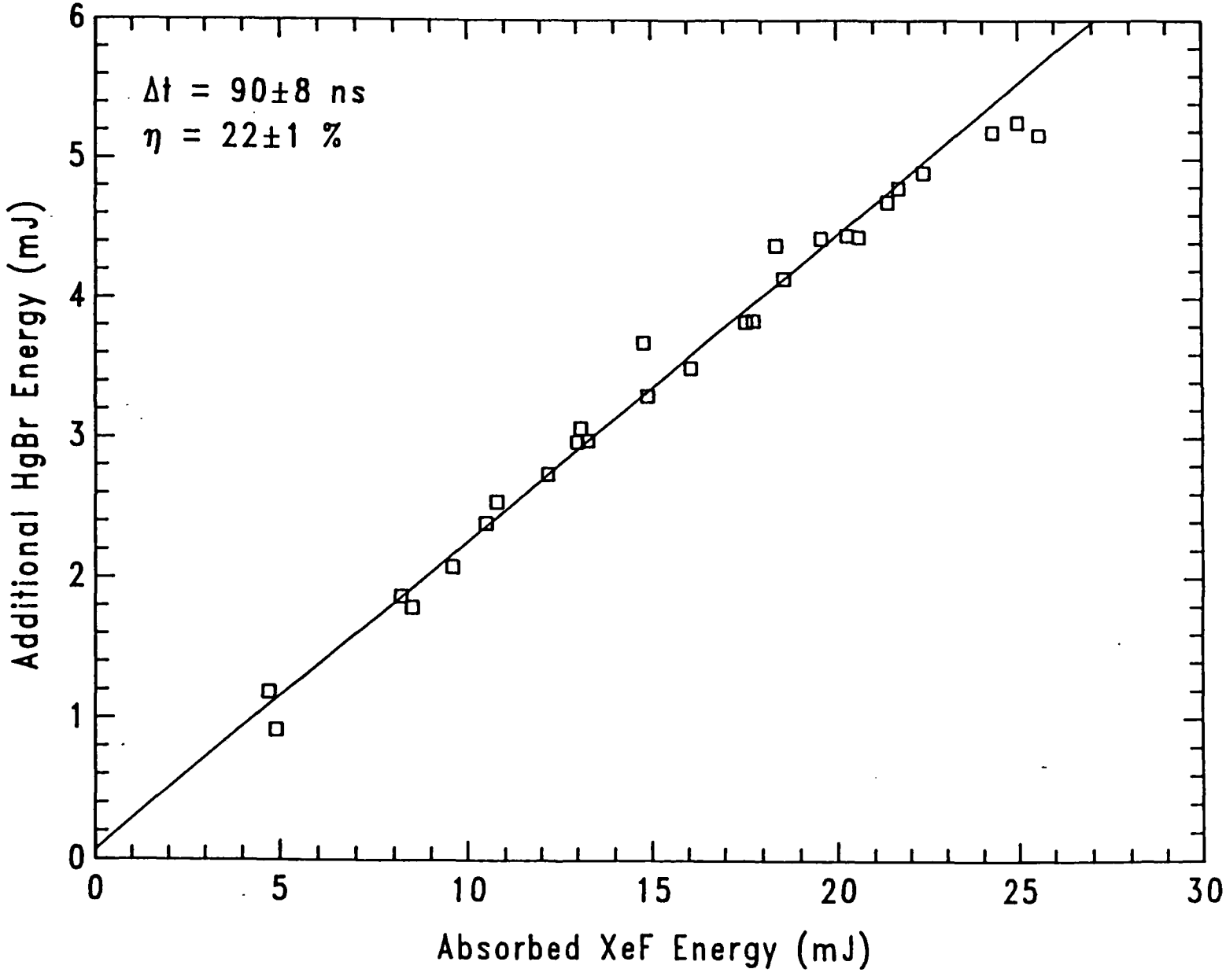
Δt = 90±8 ns
η = 22±1 %
Additional HgBr Energy (mJ)
Absorbed XeF Energy (mJ)
0
1
2
3
4
5
6
0
5
10
15
20
25
30

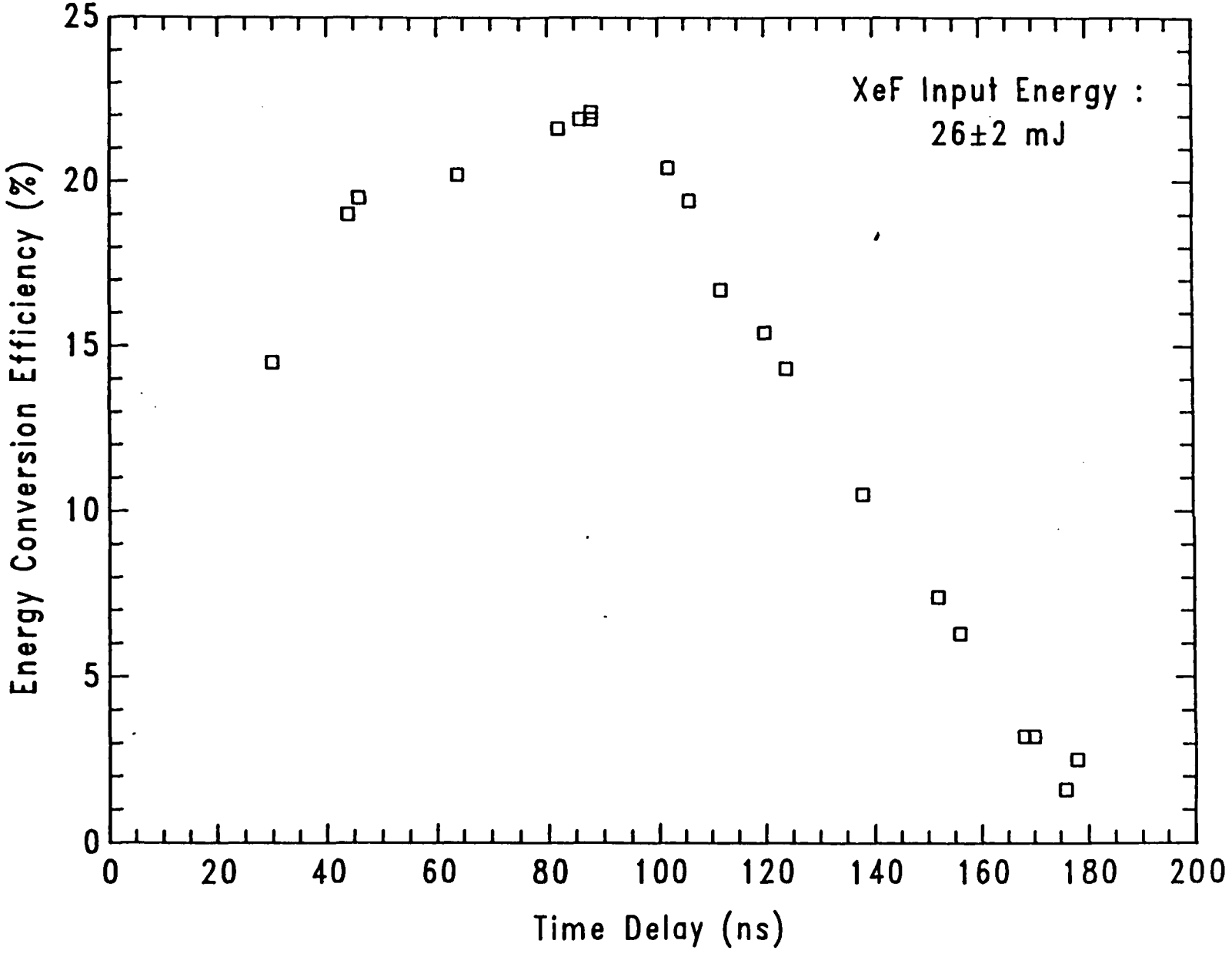
XeF Input Energy :
26±2 mJ
Energy Conversion Efficiency (%)
Time Delay (ns)
0
5
10
15
20
25
0
20
40
60
80
100
120
140
160
180
200

END

2-87

DTIC